

Development of a Catheter Stabilization Device for Stent Placement Aid

by

Dylan Crocker

Department of Mechanical Engineering and Materials Science
Duke University

Date: _____

Approved:

Patrick Codd, Advisor

Daniel Buckland

Erik Hauck

Thesis submitted in partial fulfillment of
the requirements for the degree of Master of Science
in the Department of
Mechanical Engineering and Materials Science in the Graduate School
of Duke University

2019

ABSTRACT

Development of a Catheter Stabilization Device for Stent Placement Aid

by

Dylan Crocker

Department of Mechanical Engineering and Materials Science
Duke University

Date: _____

Approved:

Patrick Codd, Advisor

Daniel Buckland

Erik Hauck

An abstract of a thesis submitted in partial
fulfillment of the requirements for the degree
of Master of Science in the Department of
Mechanical Engineering and Materials Science in the Graduate School of
Duke University

2019

Copyright by
Dylan Crocker
2019

Abstract

The purpose of this research is to introduce a novel device to intracranial flow-diverting stent delivery in endovascular neurosurgery to limit, and potentially eliminate, issues associated with instability upon stent delivery. Precisely, the goal of the device is to initiate a friction force between the delivery system and the arterial vessel wall to both assure immediate stent deployment and prevent axial advancement of the stent-anchoring wire. A prototype was constructed and its effectiveness of applying a friction force to a vessel wall was tested *ex vivo* using an LRX Plus Materials Testing Machine. Afterwards, the experimental performance of the device was compared to that of a finite element simulated model. The device demonstrated the ability to apply a friction force to the vessel wall to meet its objective. However, experimental values were consistently greater than those gathered from the simulation. Since the force prescribed by the device is minimal, future work includes increasing the force capabilities of the device and defining force requirements. Upon further development and testing, this device can be implemented into endovascular neurosurgery to improve occlusion rates of intracranial aneurysms and reduce patient risk during these operations.

Dedication

I would like to dedicate this thesis to those who have helped me achieve my academic goals. To my family, especially my fiancé Megan, my father, grandparents, and friends, all of whom gave endless emotional and financial support and encouragement during my academic endeavors.

Contents

Abstract	iv
List of Tables	ix
List of Figures	x
Acknowledgements	xii
1: Introduction	1
1.1: Flow-Diverting Stent Placement in Endovascular Aneurysm Repair (EVAR).....	2
1.2: Motivation	5
1.3: Hypothesis.....	6
1.4: Outline of Master’s Thesis.....	6
1.5: Summary.....	8
2: Literature Review.....	9
2.1: Risks of Intracranial Aneurysms	9
2.2: Complexity of EVAR – Stent Selection and Other Complications	10
2.3 Other Methods of Aneurysm Repair	11
2.3.1: Detachable Coils	12
2.3.2: Clipping	13
2.3.3: Considerations for Technique Selection.....	14
2.4: Invention and Relevant Work.....	18
3: Methods.....	21
3.1: Design Approach.....	21

3.1.1: Basic design concept	21
3.1.2: Implementing the Design Concept	25
3.2: Design Considerations.....	28
3.2.1: Biocompatibility.....	29
3.2.2: Mechanical Considerations.....	30
3.2.3: Navigation of Stent-Anchoring Wire and Controllability	31
3.2.4: Dimensioning.....	32
3.2.5: Manufacturability.....	33
3.3: Prototypes.....	34
3.3.1: Prototype A	35
3.3.2: Prototype B.....	37
3.3.3: Prototype C - Final Prototype	38
3.4: Experiment A	39
3.4.1: Experiment A – Set Up	40
3.4.2: Experiment A with Dry PTFE.....	44
3.4.3: Experiment A with PBS 1X-Hydrated PTFE	47
3.4.4: Experiment A with PBS 1X-Hydrated Porcine Artery	47
3.5: Experiment B – Artery in Tension.....	49
3.6: Simulation A – Computer Simulated Slip Force Determination	51
4: Results.....	56
4.1: Experiment A Results	56
4.2: Experiment B Results	61

4.3: Simulation A Results.....	63
5: Discussion	68
5.1: Prototype C Construction and Effectiveness.....	68
5.2: Experiment A - Interpretation of Results.....	69
5.2.1: Comparison among Peak Forces for Various Vessels.....	70
5.2.2: Dry PTFE Vessel – Force and Displacement Curves.....	72
5.2.3: PTFE Vessel Hydrated with PBS 1X - Force and Displacement Curves.....	74
5.2.4: Porcine Artery Hydrated with PBS 1X - Force and Displacement Curves	75
5.3: Experiment B - Interpretation of Results.....	77
5.4: Simulation A - Interpretation of Results	80
5.4.1: Accuracy of the Simulation.....	80
5.4.2: Data Discussion	81
6: Conclusions.....	85
6.1: Summarization of Device Performance.....	85
6.2: Future Work	86
6.3: Value of this Research.....	89
Appendix A.....	91
References	92

List of Tables

Table 1: Comparison of aneurysm repair methods.....	18
Table 2: Comparison of experimental and simulated maximum friction forces.....	83
Table 3: Summary of considerations for further reseach.....	89
Table 4: Raw data from Simulation A.....	91

List of Figures

Figure 1: Purpose of a flow-diverting stent.....	2
Figure 2: Flow-diverting stent delivery and its components.....	4
Figure 3: Detachable coiling for intracranial aneurysm repair.....	13
Figure 4: Surgical clipping for intracranial aneurysm repair	14
Figure 5: Free body diagram of current stent delivery system during unsheathing.....	23
Figure 6: Free body diagram of current stent delivery system after unsheathing.....	23
Figure 7: Free body diagram of novel stent delivery system during unsheathing.....	24
Figure 8: Free body diagram of novel stent delivery system after unsheathing.....	24
Figure 9: Concept of curved springs to apply contact force	26
Figure 10: Free body diagram of novel stent delivery system with friction force during unsheathing.	27
Figure 11: Free body diagram of novel stent delivery system with friction force after unsheathing	28
Figure 12: First iteration prototype, Prototype A.....	36
Figure 13: Second iteration prototype, Prototype B.....	38
Figure 14: Third iteration prototype, Prototype C	39
Figure 15: LRX Plus Series Materials Testing Machine	43
Figure 16: Simplified test set up of Experiment A.....	44
Figure 17: 3D-modeled component for fixing PTFE tubing in Experiment A.....	45
Figure 18: Experiment A test set-up with 3D-modeled component for fixing PTFE tubing	45
Figure 19: 3D-printed component for fixing porcine artery in Experiment A.	48

Figure 20: Experiment A test set-up with 3D-modeled component for fixing porcine artery	49
Figure 21: Experiment B set-up for tension test of porcine artery	50
Figure 22: Prototype C measurements for Simulation A	52
Figure 23: Simulation A spring profile.....	53
Figure 24: Simulation A set-up.....	54
Figure 25: Experiment A force response – dry PTFE vessel.....	57
Figure 26: Experiment A displacement response – dry PTFE vessel.....	58
Figure 27: Experiment A force response – PTFE vessel hydrated with PBS 1X.....	58
Figure 28: Experiment A displacement response – PTFE vessel hydrated with PBS 1X..	59
Figure 29: Experiment A force response – porcine artery hydrated with PBS 1X	59
Figure 30: Experiment A displacement response – porcine artery hydrated with PBS 1X	60
Figure 31: Experiment A - maximum force distributions	61
Figure 32: Experiment B - force response of porcine artery in tension	62
Figure 33: Experiment B - calculated spring constant of porcine artery in tension.....	62
Figure 34: Simulation A - spring constant response	64
Figure 35: Simulation A - principle stress response in radial direction	65
Figure 36: Simulation A - pullout force for a two-spring device.....	66
Figure 37: Pullout force comparison between Experiment A and Simulation A.....	67
Figure 38: Experiment B - necking of porcine artery.	78

Acknowledgements

I would like to express my gratitude to my fellow members of the Brain Tool Laboratory at Duke University, most importantly Dr. Patrick Codd and Dr. Weston Ross, who provided intellectual support and mentorship throughout my studies. None of this work would have been possible without their guidance.

1: Introduction

Angioplasty is a medical imaging technique in which a fluorescent dye such as sodium fluorescein is injected into a patient's blood vessel, and then an X-ray machine is used to visualize the patient's circulatory system at several frames per second ^[32]. This allows for diagnosis of blood vessel conditions throughout the body, including those in the brain, heart, spine, and periphery. Furthermore, angioplasty is used to treat these conditions in a family of procedures known as endovascular surgery, a minimally invasive surgical process that has gained popular attention since the early 1990's. With near real-time imaging, surgeons can navigate the circulatory system to deliver the appropriate therapies to the site of interest. Common applications of endovascular surgery include delivery of ballooning stents to treat stenosis in the heart, cancer-killing drugs to eliminate tumors in the spinal cord, and stent grafts to occlude aneurysms in the heart, abdomen, and brain.

Endovascular surgery is often favored over open procedures because it poses a lower mortality perioperative risk to the patient due to its decreased invasiveness ^[16]. On the contrary, endovascular surgery is limited in its applicability and often renders the need for reintervention ^[11]. Accordingly, efforts are constantly made in the medical community to introduce improvements in endovascular surgery in terms of its long-term success rate and patient safety. For the purpose of this research, one application of endovascular surgery called endovascular aneurysm repair (EVAR) will be examined.

This research focuses on a necessary improvement of flow-diverting stent placement in intracranial EVAR to stabilize the stent delivery system and prevent underlying causes of stent misplacement and stent-anchoring wire complications.

1.1: Flow-Diverting Stent Placement in Endovascular Aneurysm Repair (EVAR)

Understanding the motivation of this research first requires an understanding of flow-diverting stent delivery as a technique to treat intracranial aneurysms. Flow-diverting stent delivery systems like the Pipeline Embolization Device (PED) are designed to redirect blood flow away from an aneurysm. In theory, when the PED is placed over the aneurysm, the lack of blood flow to the aneurysm forces it to occlude, or close, over a period of weeks to months. To visualize this interaction, Figure 1 below shows a simplification of how a flow-diverting stent is placed over an aneurysm to redirect blood flow away from it.

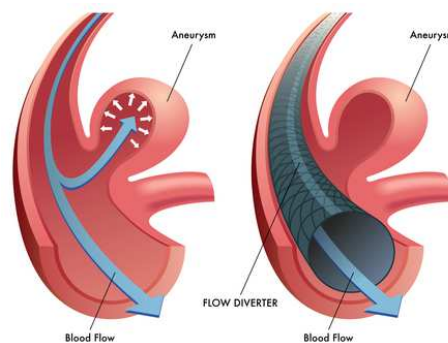


Figure 1: Purpose of a flow-diverting stent ^[20], adapted from Pegasus Therapeutics. Once the stent is placed, blood flow is redirected away from the aneurysm and the aneurysm occludes over time.

Figure 1 does not demonstrate the complicated steps leading to accurate placement of the flow-diverting stent. This process for intracranial flow-diverting stent delivery is as follows. Note that some intermediate steps that arise on a patient-by-patient basis have been excluded for simplification, and all the steps listed below are done in synchrony with angiography to locate the aneurysm.

- 1) An incision is made near the groin to access the carotid artery.
- 2) A guidewire is “advanced under fluoroscopic control ^[40],” meaning the surgeon views the angiogram while advancing the wire to visualize its path in the circulatory system. This guidewire is typically 0.035 inches, or 0.889 millimeters in diameter, and it is usually made of PTFE or nitinol.
- 3) Once the guidewire approaches branches of arteries that are too narrow for its specificity, perhaps the vertebral artery around the base of the neck, a support catheter is strung along the guidewire to hold the location and the first guide wire is removed.
- 4) A smaller guidewire, typically nitinol wire of 0.010 or 0.014 inches (0.254 or 0.3556 millimeters) in diameter is threaded through the support catheter ^[31]. This guidewire is used to navigate the intracranial arteries and find the final target location of the aneurysm. Once the location is found, the support catheter is removed.

- 5) A separate microcatheter that comes with the stent delivery system is strung along the guidewire. This microcatheter serves as the housing of the stent graft that restricts it from expanding. The guidewire is removed.
- 6) A stent-anchoring wire is introduced through the microcatheter. This wire is often extended a bit distally past the microcatheter. The surgeon gives a final check of the stent graft alignment and the microcatheter is removed. This breaks the connection between the stent-anchoring wire and the stent graft which advances the wire distally slightly, and the stent graft releases radially towards the artery wall. Figure 2 below shows the configuration of the flow-diverting stent delivery.

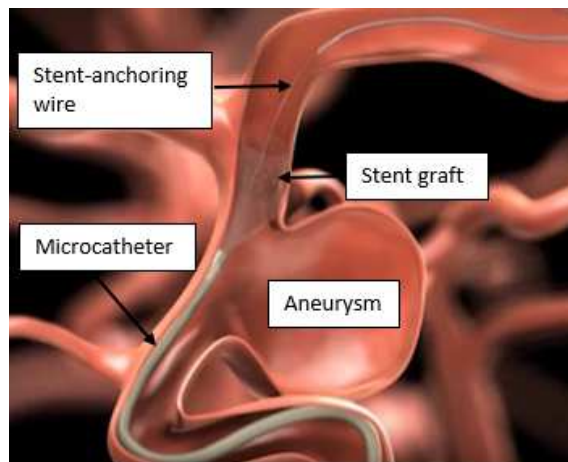


Figure 2: Flow-diverting stent delivery and its components ^[37], adapted from AtlantiCare.

- 7) Everything is unsheathed, the incision is closed, and the patient is ready to recover.

1.2: Motivation

Subject Matter Experts (i.e. neurosurgeons) were consulted, and they identified the crucial need to improve effectiveness of intracranial flow-diverting stent delivery by limiting risks associated with stent misplacement and stent-anchoring wire complications. Geographic miss is a common cause of long-term aneurysm occlusion failure, and it simply means that the stent was not placed in the exact specified location. The most common cause for this is the fact some stent grafts do not expand immediately upon retrieval of the microcatheter, so the stent needs to be dragged over the aneurysm using the angiogram display. This sounds simple, but sometimes it is not that easy. Some stents provide a higher radial force to the vessel than others depending on the size specification, so the surgeon must be very careful while dragging it. Because of this, occasionally the surgeon will have to compromise by dragging the stent to an acceptable location and not the ideal location, causing the injured segment of the vessel to not be covered completely. Other times, the surgeon will not have room to drag the stent if a bifurcation point distal or proximal to the lesion does not allow for this translation.

The principle of stent dragging forces the surgeon to advance the stent delivery system further than theoretically necessary into the vasculature. This introduces complications related to stent-anchoring wire advancement. As the stent-anchoring wire gets closer to the next bifurcation point, the likelier it is that the wire advances distally into the proximal branch of arteries, increasing the risk of vessel perforation, wire

induced embolization, and knotting or looping of the wire. Accordingly, there is a critical need in EVAR to stabilize the stent-anchoring wire and restrict its distal advancement upon retrieval of the microcatheter to limit wire complications. There is also a need to initiate stent graft deployment immediately upon retrieval of the microcatheter to limit geographic miss.

1.3: Hypothesis

The hypothesis addresses these two major issues associated with flow-diverting stent delivery. It suggests that inducing a friction force between the stent-anchoring wire of the delivery system and the arterial wall will allow the stent to be placed accurately upon unsheathing without unwanted translation and restrict the stent-anchoring wire from advancing after unsheathing the stent. This work entails the development of a novel device incorporated into the stent delivery system that addresses these two major complications by fixing the stent-anchoring wire to the vessel wall upon stent delivery without rupturing the vessel. This invention restricts stent-anchoring wire advancement and provides relative force between the stent-anchoring wire and the microcatheter, allowing the stent graft to expand immediately.

1.4: Outline of Master's Thesis

This Master's thesis is assembled in the following manner:

- Chapter 2: Literature Review – the purpose of this chapter is to give the reader an idea of the related work from which this thesis protrudes. This chapter will introduce:
 - The risks of intracranial aneurysms
 - A further look into other methods of intracranial aneurysm treatments and their associated outcomes, including comparisons between different techniques, and considerations for using each technique
 - Relevant patents that have attempted to address the complexity of stent delivery stabilization
- Chapter 3: Methods – the purpose of this chapter is to describe the design approach that addresses the critical need. This includes the design process, creation of the prototype, and the series of bench-top tests that demonstrate the effectiveness of the design. The construction and experiment of a computer simulated model will also be addressed.
- Chapter 4: Results – this chapter explains the results of each experiment and introduces analyses to evaluate these results as they compare to the hypothesis. Furthermore, a comparison between computer simulated results and prototyped experimental results will be established.
- Chapter 5: Discussion – this chapter provides an in-depth discussion on the experimental and simulated results of the research and offers reasoning for

differences between approaches. Additionally, this chapter will briefly discuss manufacturability of the design and how the prototype compares to the proposed manufactured model.

- Chapter 6: Conclusions – this chapter not only summarizes the work, but it also offers recommendations for improvement on the work that was conducted. Furthermore, it discusses possible alternative applications and the future work necessary to refine the design and market the product.

1.5: Summary

This research focuses on the development of a stabilization device as an alternative to the stent-anchoring wires currently used in flow-diverting stent delivery systems. Throughout this thesis, a design is presented that has been developed to address the critical need. This design was prototyped and tested in a series of realistic circumstances to prove its effectiveness if it were to be implemented in practice. Be mindful that the design does not solely regard stents and their capabilities. Moreover, it addresses the need for precision placement and restriction of distal advancement of the stent-anchoring wire. Thus, this work could be adapted to meet the needs of various stenting procedures, and this paper will introduce some of those possibilities in the Conclusions chapter.

2: Literature Review

This chapter is intended to provide the reader with background knowledge in the field of aneurysm repair. First, some of the risks of intracranial aneurysms according to credible studies will be introduced. Next, the complexity of EVAR will be discussed in further detail, outlining the vast stent market and other issues associated with flow-diverting stenting procedures. Other methods of aneurysm repair will then be discussed in detail, comparing advantages and disadvantages of each along with considerations for technique selection. Lastly, the chapter will conclude with a brief explanation of the invention approach, followed by a look into relevant work that has the same motivation as this research. The shortcomings of previous work will be noted as well as the distinction between previous technical approaches and this current approach.

2.1: Risks of Intracranial Aneurysms

Aneurysms pose a dangerous risk to victims. In fact, a large retrospective study from 2017 found that the combined neurological morbidity and neurological mortality rate as a result of intracranial aneurysms is 7.1 percent ^[18]. This means that 7.1 percent of patients suffering from an intracranial aneurysm will at least have lasting brain damage. An aneurysm is simply a weakening of the artery wall causing a localized bulge in the vessel. When left untreated, an unruptured aneurysm can become large enough to compress surrounding soft tissues, and when this happens in the brain, there are clear neurological effects stemming from the lesion like motor skill and speech deficits ^[30]. As

the aneurysm grows, it increases the risk of rupture. A ruptured aneurysm is even more detrimental as it leads to hemorrhage that often results in ischemia, an insufficient blood flow resulting in necrosis, or permanent cell death, of surrounding tissues ^[30]. These surrounding tissues are often vital organs or critical cerebral areas. Thus, intracranial aneurysms must be treated quickly and effectively to assure patient safety.

2.2: Complexity of EVAR – Stent Selection and Other Complications

Despite the tremendous developments in the field of EVAR, challenges still exist even beyond considerations for the motivation of this work. Another prominent challenge is a somewhat all-encompassing one, and it is the principle that patients can carry conditions that present challenging anatomy ^[13]. Some examples of these are angulated proximal neck aneurysms, Iliac Disease in which an artery is obstructed, and the complex branching network of arteries ^[13]. Typically, the anatomical challenges require the surgeon to introduce other means of intervention. In the Iliac Disease example, the surgeon may vary the access point to another artery or bypass an artery with a complicated route ^[13]. With proximal neck aneurysms, the surgeon often deploys multiple stents over the aneurysm to assure occlusion, which requires the second stent to be placed partially within the first stent ^[13], a technique that can be very cumbersome and tedious.

As one might imagine, stent delivery is a complicated segment of aneurysm repair since there are many variables of aneurysm anatomical characteristics that arise on a case by case basis. While this research does not pertain to stent design and selection, it is important to note the extensivity of stent products that meet a wide range of needs. The stent market is tremendously dense with countless products, including the Medtronic Pipeline Flex Embolization Device, the Medtronic Resolute Integrity DES, and the Stryker Surpass Device. There are carotid stenting procedures in which a ballooning catheter is used to deliver a stent graft at a point of stenosis in the carotid artery to increase blood flow rate by providing a radial force to the artery ^[39]; there are branching stents used in aortic aneurysms located near side branches to redirect blood flow ^[23], and so on. Stent delivery system development and stent manufacturing both require extensive knowledge and research to meet all patient needs. However, this research pertains to flow-diverting stent placement and not stent selection itself.

2.3 Other Methods of Aneurysm Repair

Aside from EVAR, there are several other options of aneurysm repair in practice. The two most common are detachable coiling and surgical clipping. All these procedures have their strengths and weaknesses. Additionally, none of the procedures outlined here can be used perpetually. There are certain guidelines for determining which technique is the most appropriate for treating the aneurysm on a case by case

basis. The following subsections explain these other procedures and considerations for technique selection.

2.3.1: Detachable Coils

Another common method of intracranial aneurysm treatment is detachable coils. There are several models of detachable coils (Guglielmi coils, Matrix coils, etc.), but they all operate similarly. Detachable coils involve much of the same process as flow diverting stent delivery. However, there are some key differences between the procedures. Detachable coils work on the principle of electrolysis. The distal end of a stainless-steel wire is soldered to a soft platinum coil. Platinum has a higher thermal resistance than stainless-steel, and this is very important to the operating principle. When a current is applied to the proximal end of the stainless-steel wire, its distal end is separated from the platinum coil, leaving the platinum coil to detach from the stainless-steel wire ^[24]. In practice, the microcatheter is positioned coaxially through a support catheter with its distal end in the aneurysm sac itself. The stainless-steel wire with the detachable platinum coil is then advanced coaxially through the microcatheter. Next, a small current of 1 to 1.5 milli-amps and 2 to 3.1 milli-volts is applied to the proximal end of the stainless-steel, inducing complete separation of the platinum coils into the aneurysm sac within minutes ^[24]. Lastly, the stainless-steel wire, microcatheter, and support catheter are unsheathed from the patient. Figure 3 below provides a much-needed visualization of this technique.

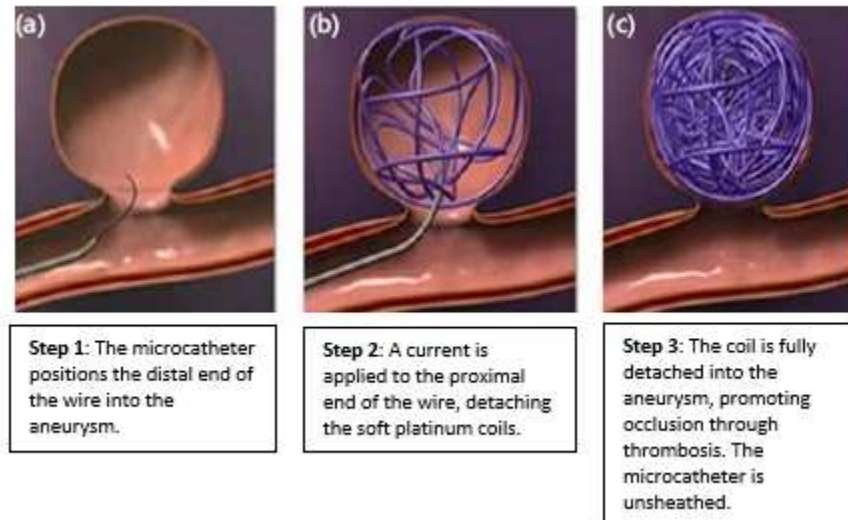


Figure 3: Detachable coiling for intracranial aneurysm repair ^[9], adapted from Platinum Metals Review.

The purpose of this technique is to promote thrombosis, or local coagulation, within the aneurysm and severely restrict blood flow to the aneurysm, resolving the lesion. Occasionally, after the coiling procedure, a loose-meshed stent is placed across the neck of the aneurysm to restrict the coils from drifting into the artery.

2.3.2: Clipping

Another approach to intracranial aneurysm repair is surgical clipping, and it is certainly the most primitive. In fact, clipping is not an endovascular procedure at all. This procedure is performed under general anesthesia. The surgeon removes a small piece of the skull in what is called a craniotomy to locate the aneurysm. This often requires the surgeon to manipulate his or her way around the brain while practicing great care as to not damage the brain. Once the aneurysm is accessed, the surgeon places

a spring-loaded titanium clip at the base of the aneurysm neck to segregate it from the artery. Figure 4 below shows a simplified visual of surgical clipping.

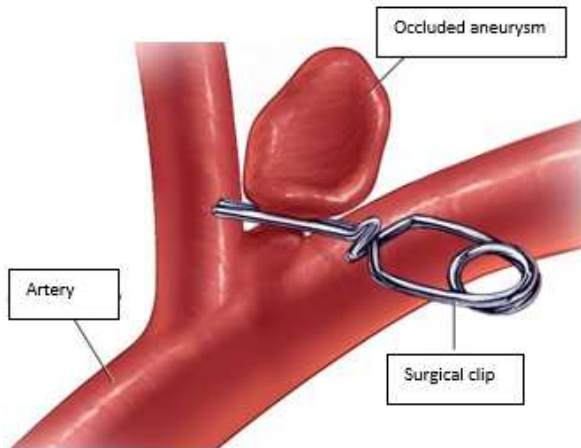


Figure 4: Surgical clipping for intracranial aneurysm repair ^[2], adapted from the Mayo Clinic.

As seen in Figure 4, the clip eliminates blood flow into the aneurysm which forces it to occlude over time ^[25]. Once the task is complete, the clip is left in place. Clipping is also used on ruptured aneurysms to terminate hemorrhaging.

2.3.3: Considerations for Technique Selection

Like any surgical procedure, none of these techniques are used ceaselessly. There are circumstances that require the utilization of certain techniques, and there are circumstances that prohibit others. This section outlines the advantages and disadvantages of the three intracranial aneurysm treatment techniques previously established and provides insight on considerations for method selection in practice.

Endovascular surgery is often favored over open procedures because it poses a lower mortality perioperative risk to the patient due to its decreased invasiveness ^[16]. Flow-diverting stents are typically used to treat intracranial aneurysms when anatomical location of the lesion poses an issue in accessibility, making clipping difficult to perform. Additionally, stenting can be used to treat any aneurysm regardless of its characteristics. For example, wide-necked aneurysms may deem coiling an inappropriate therapy ^[38], but a stent can be used as an effective substitute. This is possible because there are dozens, if not hundreds, of stent products of various sizes, so there is always a stent that fits. In some extreme cases of wide-necked aneurysms, two stents can be placed in series with one another to divert blood flow away from the aneurysm. Altogether, this characteristic makes flow-diverting stent placement the most versatile of treatment techniques. On the contrary, endovascular surgery is limited in its applicability and often renders the need for reintervention ^[11]. Accordingly, efforts are constantly made in the medical community to introduce improvements in endovascular surgery in terms of its long-term success rate and applicability.

Moreover, stent placement and detachable coiling are performed in a catheterization lab, which is beneficial in the following regards. First, the patient is administered sedatives and sometimes local anesthesia instead of general anesthesia, which is used in the operating room where clipping is performed. The administration of general anesthesia in the operating room can pose a risk of pulmonary, cardiac, and

central nervous system complications, among others, especially for elderly patients ^[21]. Secondly, catheterization lab procedures are more cost efficient for hospitals since they do not require some of the necessities of the operating room, like endotracheal intubation and intensive hemodynamic monitoring ^[4]. The catheterization lab allows hospitals to endure a lower cost without compromising patient safety. Thirdly, due to the invasiveness of the procedure, clipping requires a longer recover time than coiling or stenting. Clipping patients are often monitored for days, even up to a week or more in the hospital after the procedure, while stenting and coiling patients typically spend a day or two in the hospital before returning to normal activity after about a week.

Flow-diverting stenting is the least effective treatment for intracranial aneurysms. The procedure holds a higher percentage of long-term aneurysm occlusion failure and requires more revision procedures than clipping and coiling. Coiling is a middle ground between stenting and clipping, offering intermediate long-term effectiveness, while clipping is the most effective aneurysm therapy among the three. A retrospective cohort study found that among 29 aneurysm cases treated with flow-diverting stenting, about 20 percent failed to occlude after 9 months ^[38]. This nearly agrees with another study that claimed out of 178 intracranial aneurysms treated with stenting, 19 percent failed to occlude after 12 months ^[41], so we can believe this failure rate as credible. While it is unclear in either study how many cases required revision surgery, we can infer that an aneurysm that has failed to occlude likely required a

revision surgery. So, while the revision surgery rates may not be equivalent to the occlusion failure rates, they are certainly positively correlated. A retrospective cohort on clipping and coiling found that only 3.8 percent of clipped aneurysms required revision surgery compared to 17.4 percent of coiled aneurysms [26].

In addition, stent delivery brings potential complications associated with wire advancement. Upon retrieval of the microcatheter, which releases the stent graft and breaks the bond between the stent graft and the stent-anchoring wire, this undesirably advances the stent-anchoring wire, which can be a critical issue at bifurcation points in the vasculature as it can cause perforated arteries, embolization due to breakage of the distal tip of the wire, and looping or knotting of the wire [19].

Despite the favorable success rate of clipping, it is only used when the aneurysm is accessible. Given the procedure details, this makes sense because the surgeon must handle the brain to expose the artery. If the aneurysm is located deep within the brain, the surgeon will likely face a complicated path of navigation. When the surgeon navigates the brain with surgical tools, there is always the risk of permanent insult to the brain. The invasiveness of the procedure suggests that the more the surgeon must navigate, the greater the risk of permanent insult. Thus, aneurysms near the surface of the brain or those that have an accessible path are most treatable with clipping. Table 1 below provides a much-needed concise summary of the comparison between treatment selection for treating intracranial aneurysms.

Table 1: Comparison of aneurysm repair methods

Treatment Selection	Pros	Cons	Complication Rates	Conditions where treatment is optimal	Conditions where treatment should be avoided
Clipping	Most effective	Invasive, performed in OR (anesthesia, longer recovery, etc.)	3.8% [26]	Easily accessible aneurysms (i.e. near the surface of the brain)	Challenging anatomical location
Coiling	Performed in catheterization lab (no anesthesia, cost efficient, quick recovery)	Additional stenting to contain coils, not ideal for aneurysms with challenging characteristics (i.e. wide neck)	17.4% [26]	Challenging anatomical location but not challenging anatomical characteristics	Since less effective than clipping, clipping should be considered first if possible
EVAR	Versatile, performed in catheterization lab (no anesthesia, cost efficient, quick recovery)	Least effective, wire complications (knotting, perforation, etc.), risk of reintervention	19 - 20% [38][41]	Challenging anatomical location and challenging aneurysm characteristics	Since least effective, other treatments should be considered first if possible

2.4: Invention and Relevant Work

The invention is comprised of a stent-anchoring wire with compressible, medical grade nitinol springs at its distal end that would replace the standard stent-anchoring wires within stent delivery systems. The distal ends of both the microcatheter and stent-anchoring wire align. The springs are compressible so that they can be contained within

the microcatheter until stent deployment. Upon stent deployment, as the microcatheter is retrieved, the springs expand radially, providing a normal force to the artery wall without rupturing it. The spring gives a bi-directional friction force to oppose both the axial force placed on the microcatheter by the surgeon and axial advancement of the wire, thus addressing the critical need. The microcatheter is then advanced axially to contain the springs again and the entire system is unsheathed. A deeper explanation of the design will come in Chapter 3 where sketches and images of the prototype will be provided, along with reasoning for material selection.

Several companies have attempted to address the issue of geographic miss and guide wire complications, but none have taken the approach of this design. Competing companies of this technology include global medical companies Medtronic and Stryker, and Route 92 Medical, a small start-up in Silicon Valley. Route 92 Medical holds the most competitive design as outlined in U.S. Patent Number 20180242978A1 ^[7]. This invention is a tethering device for endovascular surgery that advances an anchor distally and deploys it within a nearby branching vessel. While this is a clever idea, it is never desirable to advance into the vasculature further than necessary, and this makes re-sheathing the system difficult too. The branched vessel could be narrower than the target vessel of the lesion, so introducing the microcatheter into the neighboring vessel could be dangerous as a stagnation of blood flow could occur. Medtronic and Stryker have addressed the issues by incorporating re-sheathable and more easily deployable

stent grafts. This allows the surgeon to reposition the stent if the initial placement is not acceptable. This is a good idea too, but it does not solve the issue of unnecessary guide wire advancement. Ultimately, the design proposed in this research is unique and addresses the full extent of current limitations without compromising patient safety.

3: Methods

This chapter describes the methods and approaches, from start to finish, relating to all aspects of this research. Included are discussions of the need assessment, design approach and iterations, the creation of the device, and tests and simulations conducted to demonstrate its effectiveness. Also included is an explanation as to why these tests are necessary, and how the results will play an important role in future work. The results and analyses of these tests will be discussed in future chapters.

3.1: Design Approach

The design of the invention was certainly an iterative process. I spent several weeks at the beginning of my Master's program assessing the needs within the endovascular space. Several visits were paid to Duke Health to gain exposure to various procedures with the goal of determining which problems can be solved from an engineering standpoint. While witnessing a flow-diverting stenting procedure to treat an intracranial aneurysm, a surgeon pointed out the need to stabilize the stent-anchoring wire upon delivery of the stent graft. From there, design considerations were researched in parallel while brainstorming design principles until the seemingly optimum design was achieved.

3.1.1: Basic design concept

Geographic miss and distal advancement of the wire can be limited, or ideally eliminated, in one global manner: a force must be introduced to refrain the wire from

advancing while unsheathing the stent, and another relative force must be introduced between the stent graft and the microcatheter to allow the microcatheter to unsheath. In theory, it is really that simple. The difficult part is applying that force *in vivo* within a complex vasculature path of minute vessels. Another consideration that makes this application of force challenging *in vivo* is the actuation of force that is required at a distance far from the application point. Since the stent graft is initially fixed to the stent-anchoring wire, the wire is a key component in creating relative force between the stent graft and the microcatheter. Applying an axial force to the stent-anchoring wire in return applies the same force to the stent graft in the same axis. Considering the nearby anatomy with this procedure, the force needed for each feat can be accomplished with friction. If a device fixed to the stent-anchoring wire can apply a radial force to the artery wall, this introduces a bi-directional friction force, which both opposes the force of the stent-anchoring wire during its advancement and opposes the force of the microcatheter upon unsheathing to release the stent graft. Ideally, this friction force should be large enough to fix the wire and the stent graft in their axial locations so that the stent graft is released accurately in place while the microcatheter is unsheathed and the wire does not advance. To simplify the force interactions, it helps to look at free body diagrams of both current stent delivery systems and the novel approach. Free body diagrams of the existing stent delivery system in two stages, immediately after the surgeon begins to

unsheath the stent graft (Figure 5) and immediately after the stent is unsheathed (Figure 6), are shown below.

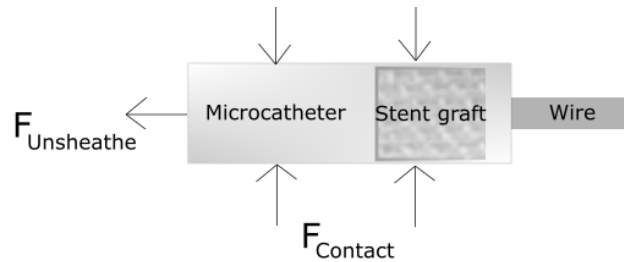


Figure 5: Free body diagram of current stent delivery system during unsheathing. The unsheathing force is applied by the surgeon during stent delivery, and the force is opposed only by contact forces. There is a contact force between the microcatheter and vessels due to bends in the circulatory system, and between the stent graft and the microcatheter. These contact forces amount to friction forces.

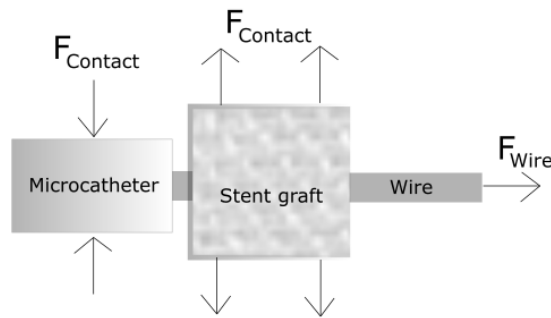


Figure 6: Free body diagram of current stent delivery system after unsheathing. The microcatheter has been pulled back and the stent graft expands. When it expands, the fixation point between the stent and the wire is broken, and this advances the wire with a force denoted as the wire force. The stent now applies a contact force to the vessel wall, which amounts to a friction force, preventing it from displacing. There is still contact between the microcatheter and the vessel wall, but the issue of microcatheter unsheathing is eradicated at this point.

The novel approach introduces a friction force that results from device contact with the vessel wall. This acts to oppose the unsheathing force seen in Figure 5 and the wire force seen in Figure 6. The way this friction force is applied will be addressed later in this paper, but Figures 7 and 8 below demonstrate conceptual free body diagrams of the novel approach in the same two stages as Figures 5 and 6.

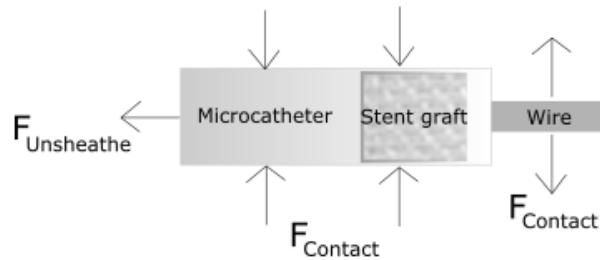


Figure 7: Free body diagram of novel stent delivery system during unsheathing. The contact force between the wire and the vessel wall introduces a friction force that opposes the unsheathing force.

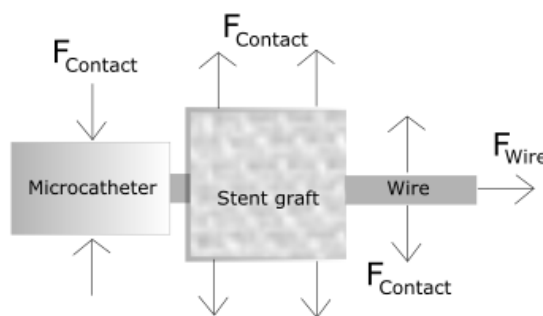


Figure 8: Free body diagram of novel stent delivery system after unsheathing. The contact force between the wire and the vessel wall promotes a friction force that opposes the wire force.

It should now be clearer from the previous figures how introducing contact between the stent-anchoring wire within the stent delivery system and the artery wall creates a friction force that both opposes the unsheathing force and the wire force. These in turn allow for immediate unsheathing upon retrieval of the microcatheter and restriction of stent-anchoring wire advancement after unsheathing, respectively. The next section, Section 3.1.2, will discuss how this friction force between the stent-anchoring wire and artery wall is addressed with the novel design.

3.1.2: Implementing the Design Concept

One simple way that the stent delivery system can apply this contact force between the stent-anchoring wire and the vessel wall is through a series of curved springs attached to the wire. This is the concept that was employed in each design iteration. Each individual curved spring carries a spring constant that is proportional to its force output. When displaced beyond its resting curvature, the spring applies a force to the vessel wall that is described by Hooke's Law shown below.

$$\mathbf{F} = k\mathbf{x}$$

X in this case is the radial displacement of the spring in forced compression dictated by the artery wall. That is, the geometry of the artery wall forces the spring into compression to generate a force. The force scales proportionally to the number of springs because the spring constant k increases linearly as springs are added. For example, if one spring has a spring constant k, using two springs will have a spring

constant of twice k , which means the force is doubled. However, it is important to note that this assumption only holds true if the springs are assumed to be identical and the system is symmetric, meaning that the springs displace the same amount. Figure 9 below illustrates this design concept and shows the series of two springs compressed mildly within the artery.

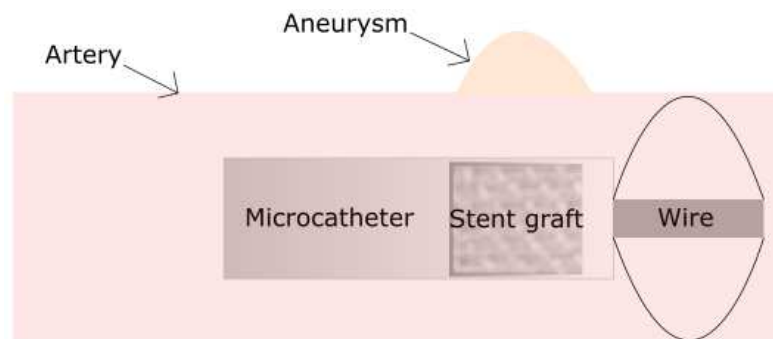


Figure 9: Concept of curved springs to apply contact force between wire and artery wall.

These springs also create contact between the stent-anchoring wire and the artery wall once the stent graft is unsheathed (refer to Figure 6). In either case, it should be obvious that since the springs contact the artery wall, the spring force results in a normal force on the artery wall. This means there is a friction force between the artery wall and the springs that opposes axial motion within the system, and this force is given by the following equation.

$$F_f = F_n \mu_s$$

The normal force is dependent on the static coefficient of friction μ_s between the two surfaces. The coefficient of friction can also be kinetic where the kinetic coefficient of friction is labeled μ_k and describes the friction coefficient between two surfaces with relative motion between them. Now, with a better understanding of how this friction force is created, Figures 10 and 11 below show free body diagrams of both the unsheathing stage and the post-unsheathing stage to demonstrate how the friction force acts within the system. The contact forces between other components of the stent delivery system and the vasculature are ignored for simplicity.

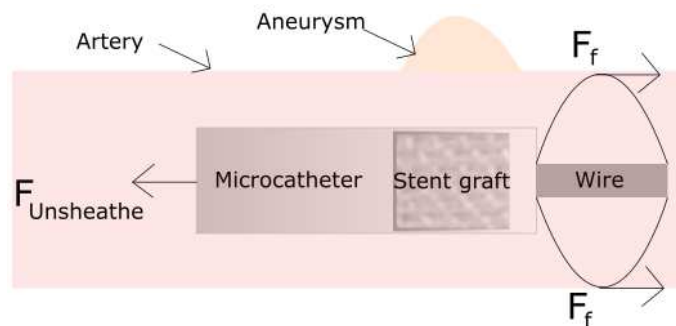


Figure 10: Free body diagram of novel stent delivery system with friction force during unsheathing. Components are not drawn to scale.

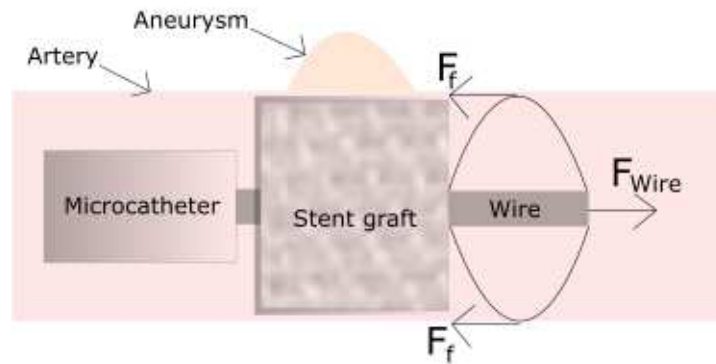


Figure 11: Free body diagram of novel stent delivery system with friction force after unsheathing. Components are not drawn to scale.

This subsection and the one prior have shown crude simplifications of the designed device to give the reader a better understanding of how the design concept addresses the need. More design criteria and considerations will be discussed in the next subsection, but this discussion of force interactions is critical to understand the purpose of the novel device in the first place. Figures 5 through 11 should be referred to throughout the reading if the reader struggles to connect these design concepts to later discussions.

3.2: Design Considerations

The design considerations with the development of this device are quite extensive. The device needs to be effective while also considering the patient's safety and health. The following subsections highlight the design considerations where they are grouped by category. Note that this section is intended to inform the reader of the design considerations of the device should it reach the market and be used in practice.

3.2.1: Biocompatibility

An obvious consideration is that the spring needs to be comprised of a biocompatible material like the rest of the stent delivery system. If it is not, the patient could have an immune response to the invasive material. There are plenty of medical grade materials that can meet the requirement of this application, including certain plastics and metals. A few examples of biocompatible metals are titanium, nickel, stainless steel, cobalt chromium molybdenum, and titanium alloys such as nitinol [3]. Examples of biocompatible plastics are polytetrafluoroethylene (PTFE), polyether ether ketone (PEEK), polypropylene, and polyurethane [15]. In addition, the springs will need to be fixed to the stent-anchoring wire somehow. Two possibilities to accomplish this are micro-soldering or using an adhesive, and both can be done while meeting the biocompatibility requirement. Biocompatible adhesives most often include epoxies and silicones that are inert and non-toxic [6]. Micro-soldering is more complicated and difficult to achieve, and it is less cost efficient given the materials that need to be used *in vivo*. Most soldering materials contain lead which is toxic, so the key is that a lead-free soldering material would need to be used [35]. Furthermore, the soldering material needs to be very fine to perform precision soldering of such small structures. Examples of solders that are both biocompatible and available in very small diameters (beginning at 0.001 inches) are eutectic gold tin (AuSn) and tin silver (SnAg) [35].

Lastly in the biocompatibility category is that the springs cannot occlude the artery. Appropriate blood flow through the artery needs to be maintained so that all parts of the brain receive the necessary blood supply. Otherwise, portions of the brain are deprived of oxygen and brain damage can occur almost instantaneously. If the artery is occluded by the springs, this can also increase the pressure proximal to the device, which can result in hemorrhaging. As previously stated, the number of springs can be scaled to meet the friction force requirement of the system, but an excessive amount of springs cannot be used. The upper limit of the number of springs will be the point at which the artery still carries acceptable blood flow.

3.2.2: Mechanical Considerations

The device needs to meet mechanical requirements. In reference to Figures 10 and 11, with an understanding of force summations, the friction forces generated by each spring must collectively sum to be equal to or greater than the unsheathing force and the wire force independently to meet the ideal criteria of completely stabilizing the system in the axial direction. The overall friction force depends on the static friction coefficient between the spring material and the artery, and this data is published in previous literature with some materials ^{[8][14]}. The number of springs and the resulting normal force provided to the artery by the springs are also important factors. These variables need to be optimized in relation to each other to generate the appropriate friction force.

Conversely, in optimizing the friction force, the radial stress that the artery wall is subject to must remain under the arterial yield stress. The yield stress is the stress at which the artery wall deforms indefinitely. Consequently, if the yield stress is reached, the artery wall would weaken, or in extreme cases, even rupture. Radial stress is dependent on the spring force and the area of contact between the spring and the artery. Ideally, these two features need to be controlled such that the radial stress of the artery is under its yield stress. Additionally, the principle stress of the spring in the radial direction cannot exceed its flexural strength throughout any step of the stent delivery process. This includes during navigation through the microcatheter and during the force application of the springs to the artery. If the flexural strength is surpassed, the springs will deform indefinitely or break. If they deform indefinitely, the spring curvature would be disrupted, and the spring force would deviate from its expected value as a result. If the spring breaks, this would be severely detrimental to the patient. This could cause a brain embolism which occurs when a foreign body disrupts blood flow within the vessels of the brain. A potential ramification of a brain embolism is an ischemic stroke, which can be life threatening or cause lifelong disability.

3.2.3: Navigation of Stent-Anchoring Wire and Controllability

With the springs attached to the distal end of the stent-anchoring wire of the stent delivery system, the springs cannot alter the navigational capabilities of the wire in any way. This means that the stent-anchoring wire needs to advance axially through the

microcatheter without damaging either the springs or the microcatheter. Microcatheters are made of durable plastics like polyurethane and polyethylene, so it is unlikely that the microcatheter would tear during the advancement of the wire. Nonetheless, the distal end of the wire should be free from obstruction so it can navigate freely throughout the microcatheter. Furthermore, with this design, the distal end of the wire is advanced beyond that of the microcatheter to deploy the stent. The stent-anchoring wire with the springs attached must be re-sheathable once the stent is deployed. The microcatheter needs to advance axially relative to the stent-anchoring wire to contain the springs once again. Once the springs are re-sheathed, the whole system can be unsheathed without dragging the springs along the entire path of the vasculature. Re-sheathing the springs might sound difficult, but the wire and the microcatheter can be controlled independent of one another, and the microcatheter can advance through the center of the stent graft once it is deployed, making this process feasible.

3.2.4: Dimensioning

Dimensioning is critical to the effectiveness of the device. The arterial inner diameter will determine how much the springs deflect, which in turn determines the spring force. The spring force in theory would increase as the artery diameter gets smaller, so smaller diameter arteries should be able to support higher unsheathing and wire forces given one specific spring. However, it is not likely that one specific spring would be able to apply the appropriate friction forces for all artery sizes. Larger arteries

would require a larger spring radius to meet the force requirements. The practical application is that a spring would be designed for a range of artery diameters. Even with this variability though, dimensions of current stent delivery systems should be considered no matter the size of the target artery. For example, a typical inner diameter of microcatheters used for intracranial stent delivery is 0.27 inches ^[36], and these typically have a maximum wire compatibility of 0.010 or 0.014 inches in diameter ^[31]. So, with the springs fixed to the wire, the springs must be designed such that the microcatheter can support the wire and the compressed springs. Dimensions of stent delivery systems scale with target anatomical locations, so the device would scale accordingly should it be used in practice for a range of applications.

3.2.5: Manufacturability

Finally, the device needs to be manufacturable. A device can be elegantly designed, but if it cannot be manufactured, there is no use for it in practice. Since the novel stent delivery system utilizes existing products, these overlapping parts used in existing products can be manufactured with certainty. The only addition with the novel design is the curved springs. Section 3.2.1 introduced the idea that the springs can be fixed to the stent-anchoring wire with adhesives or micro-soldering. Adhesives can be applied using precision application products. One such example of these devices is the PL100EPi by Nautilus Systems ^[33]. This precision applicator can apply an adhesive to components with a tolerance of 0.004 inches ^[33], which is acceptable given that the

diameter of the wire that the spring needs to adhere to is 0.010 inches. All the biocompatible materials suggested for spring materials are available in fine diameters. Additionally, some of the metals suggested, like nitinol and other titanium alloys, can be shape set. This is essentially a process where the wire is wrapped around a fixture that defines its curvature, and the wire is heated in place to hold this shape ^[12]. This would be a favorable process for manufacturing the curved springs before adhering them to the stent-anchoring wire.

3.3: Prototypes

Several prototypes were constructed to demonstrate design functionality. Some design constraints discussed in Section 3.2 need not be addressed during prototype construction since the prototype is only used to demonstrate the function of the design. Similarly, the prototypes are by no means expected to look like a finalized product. They were constructed by hand, and shall this product reach the market, it would be outsourced or manufactured using technologies and companies with the appropriate capabilities. The prototype was iterated several times until the constructed device modeled the final design most accurately. However, each design operates on the same principle laid out in Section 3.1. There are three prototypes that will be introduced, beginning with the first and ending with the latest design. The latest prototype was used to conduct experiments to demonstrate the effectiveness of the device.

3.3.1: Prototype A

This original prototype uses a wire concentric with an outer tube in place of the stent-anchoring wire in flow-diverting stent delivery systems. The outer tube is hollow, so the inner wire can translate axially within it, and the inner wire extends beyond the outer wire by about an inch. This design suggests that the stent would be anchored to the outer tube until the microcatheter is unsheathed, deploying the stent. The curved springs, made of 0.010-inch diameter nitinol, were pre-shaped by hand and are fixed to the distal end of both wires using a twine knot secured with Gorilla Glue epoxy. The outer tube is polyimide tubing of 0.072 inches in inner diameter. The inner wire is stainless-steel wire of 0.038 inches in diameter. This was considered close enough to 0.035 inches, the diameter of guidewires used in the early navigation stage in endovascular surgery, and 0.072 inches is a common inner diameter of support catheters that support a maximum wire diameter of 0.038 inches [28].

Materials were selected based on availability. The inner wire and outer tube are controlled independently such that the user can retrieve the inner wire relative to the outer tube. When the distal end of the wire retreats towards the outer tube, the springs bow out which would allow them to apply a force to the artery wall. The inner wire and outer tubing can also move as one since the contact between them is fixed and both bodies are light. Pulling either the wire or the tubing lightly allows them to translate together. As a result, this system can be advanced and unsheathed from the patient.

Dimensioning was mostly ignored with this prototype. The idea was to generate a working device, and if it worked, then it could be scaled accordingly. An image of Prototype A is shown in Figure 12 below.

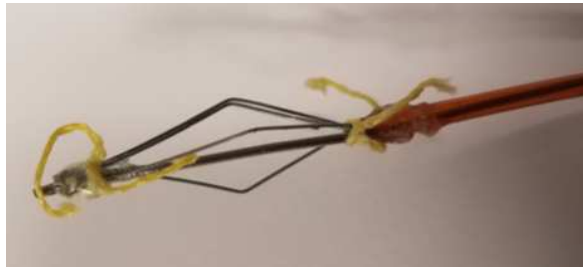


Figure 12: First iteration prototype, Prototype A. The stainless-steel inner wire passes through the orange polyimide tubing, held together with super glue and yellow twine.

After discussing this design with a Duke neurosurgeon, Erik Hauck, he suggested that it would not be possible to scale this device down to be used in practice. He said that it was not possible to introduce this system in place of the stent-anchoring wire because the clearance between the stent-anchoring wire and the microcatheter is very small to begin with. Introducing a second component would make it even tighter. Also, it would be very difficult for a surgeon to control the inner wire, the outer wire, and the microcatheter independently. It would likely take two surgeons which is not ideal. For these reasons, Dr. Hauck then suggested that the device would be more applicable if the springs could be attached to the stent anchoring wire directly. The following prototypes, Prototype B and Prototype C, were designed based off Dr. Hauck's suggestion.

3.3.2: Prototype B

This prototype takes a more simplistic approach. With Prototype B, a single wire with curved springs fixed at its distal end is used in place of the stent-anchoring wire. The stent would be anchored to this replacement wire until the microcatheter is unsheathed, and then the stent would break its bond from the wire to deploy. Again, dimensioning was mostly ignored with this prototype. Proof of concept was the goal. The wire used was the same 0.038-inch diameter stainless-steel wire used in Prototype A. The springs are made of 0.017-inch diameter polyether ether ketone (PEEK). PEEK was chosen because it is flexible, so if translated to a final product, the springs should deform easily enough to fit inside a microcatheter. Equally important, PEEK has a favorable coefficient of friction, so the idea is that the friction force will increase as a result. Most PEEK materials have a static coefficient of friction of 0.35 against steel ^[10]. In comparison, the static coefficient of PTFE against steel sits around 0.10, polyester against steel is about 0.2, and polyethylene against steel also sits around 0.20 ^[10]. Since the PEEK wire is soft, it did not have to be pre-shaped. The springs were fixed to the stainless-steel wire using Gorilla Glue epoxy. The device could be scaled accordingly should it operate favorably. An image of Prototype B is shown in Figure 13 below.



Figure 13: Second iteration prototype, Prototype B. PEEK wires are fixed to the stainless-steel wire using super glue.

Prototype B was briefly inspected for function within a PTFE tube to see if the friction force provided would be reasonable for experimentation. No formal experiment was conducted, but it was clear that the springs did not provide much force to the tubing at all. Thus, this prototype, like Prototype A, was deemed unusable, and a third prototype was constructed.

3.3.3: Prototype C - Final Prototype

This prototype is very similar to Prototype B. Curved springs are again fixed to the distal end of a wire, and this is to be used in place of the stent-anchoring wire. Nonetheless, there are some key differences between Prototype B and Prototype C. Prototype C uses a 0.010-inch diameter nitinol wire as the main wire, which is the same navigational guidewire used to access intracranial aneurysms in endovascular surgery. The springs are also made from the same wire. Dimensioning was taken into consideration with this design because this prototype was used to carry out experiments discussed in the next subsection. The springs were pre-shaped by hand and fixed to the

main wire using knots tied with copper wire, and then secured using Gorilla Glue epoxy. An image of Prototype C is shown below in Figure 14.



Figure 14: Third iteration prototype, Prototype C. Nitinol wires are fixed to the main nitinol wire using super glue and copper wire.

While Prototype B attempted to increase the applied friction force to the artery by using a material with a high coefficient of friction, Prototype C increases the friction force by increasing the spring force. It was clear upon construction that it took more force to deflect the springs in Prototype C than in Prototype B, so the spring force increased. Prototype C was also inspected for function within a PTFE tube, and it took some force to remove the device from the tubing. As a result, Prototype C was chosen as the final prototype since it generated reasonable estimated friction force.

3.4: Experiment A

To demonstrate the effectiveness of the design, Prototype C was used to conduct a bench top experiment. The experiment was designed specifically to test the hypothesis. This experiment, Experiment A, tests the slip force required to displace the prototype from its initial position within a tube to model its performance in an artery. Experiment

A was performed within dry PTFE tubing, an *ex vivo* bilateral carotid artery of a pig hydrated with phosphate-buffered saline (PBS) 1X buffer solution, and PTFE tubing hydrated with PBS 1X buffer solution. A second experiment, Experiment B, was conducted to determine the force required to tear the artery used in Experiment A. This is important because it explains how the artery itself displaces axially under tension, allowing explanation for some of the results in Experiment A. The results of Experiment A were then compared to a simulation to examine how the experimental results compare to theoretical values.

3.4.1: Experiment A – Set Up

A segment of a bilateral carotid artery was harvested from an American Yorkshire pig that had been discarded following a separate training procedure at the Duke Vivarium. No pigs were specifically acquired nor sacrificed for this study. The artery was harvested using sterile surgical tools. The bilateral carotid artery was chosen because it was easily accessible, and there is published literature that claims its dimensions. This made it easy to conduct some of the analyses. The average inner diameter of a porcine bilateral carotid artery is about 4 millimeters, or 0.1575 inches, when the pig weighs between 29 and 45 kilograms [27]. It was estimated that the sacrificed pig weighed roughly 30 to 35 kilograms, so it fell within this range. Once the artery was harvested, it was trimmed of excess biological tissue, rinsed with water, and placed in a vial filled with PBS 1X. PBS 1X was selected as the buffer solution because it

has been used in previous research to preserve porcine arteries for cellular examination^[34]. The vial was then stored in a common refrigerator at 36 degrees F for future experimentation that occurred two days later.

Before testing the prototype within the artery, I wanted to perform the experiment in a tube that roughly simulated the artery's friction properties. I did this because I did not want to damage the artery while designing the experiment. After all, I only had one arterial segment to work with. PTFE was selected as the first material to mimic the artery because PTFE and arterial tissue have a similar coefficient of static friction against nitinol, which the springs are composed of^{[8][14]}. The static coefficient of nitinol wire against common ureteral catheters has been determined by Bard Medical^[8]. While ureteral catheters are made of several different plastics, many are coated with PTFE, including Bard's PTFE Coated Latex Foley Catheters^[5]. Nitinol wire performed differently among several catheters, but the most favorable result shows that nitinol wire, when engaged with a ureteral catheter, has a static coefficient of friction of about 0.06^[8]. This may not be entirely accurate given that this catheter may not have been PTFE coated, but it is all that exists to make an educated guess.

On the other hand, a finite element analysis (FEA) of an Endostaple device assumes a static coefficient of friction between nitinol wire and the arterial wall of 0.1^[14]. An Endostaple is a device that holds a stent to the vessel wall by punching a small hole through both and secures the insertion with nitinol wire^[14]. Again, although this

assumption of the coefficient of friction between surfaces may not be perfect, it has been used as an assumption in previous research, so it is fair to define it as an educated guess. Semi-clear PTFE tubing with an inner diameter of 0.125 inches was selected for experimentation because this inner diameter is like that of the porcine bilateral carotid artery.

The idea behind this experiment was to pull the prototype from the fixed vessel, measuring the force required to induce displacement. A Lloyd Instruments LRX Plus Series Materials Testing Machine and NEXYGEN multi-stage testing software were used to conduct the experiment. The LRX Plus Series Materials Testing Machine uses a load cell of up to 5 kilonewtons to induce a specified load or displacement of a secured material ^[22]. The NEXYGEN software initiates the test, and then outputs the data onto the lab computer for data analysis. Figure 15 below shows the LRX Plus Series Materials Testing Machine that was used in Experiment A.

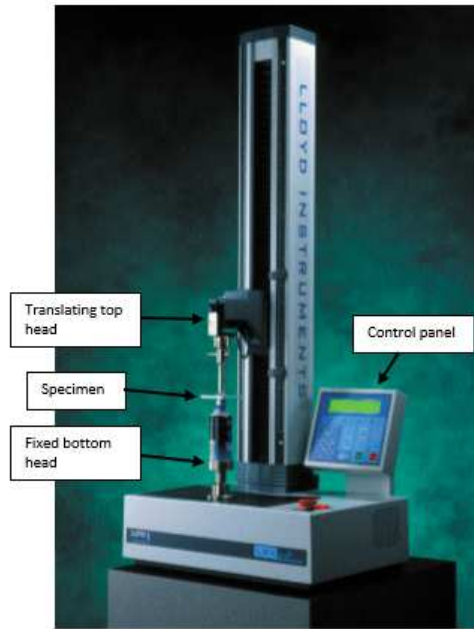


Figure 15: LRX Plus Series Materials Testing Machine ^[22], adapted from Ametek Test and Calibration Instruments. The specimen is clamped to the top and bottom heads. The top head, controlled by a load cell, then displaces at a controlled rate or applies a controlled force. The blue pad allows the user to position the top head and zero its location and force output prior to testing. The test is initiated from the lab computer (not pictured).

The LRX Plus Series Materials Testing Machine fixes the bottom end of the sample and pulls the top end. With this test, however, the tubing should ideally be fixed at both ends, and the top head of the machine should pull the prototype from the tubing to examine how much force it takes for the prototype to slip from its initial position within the tubing. These boundary conditions require three points of contact, which are not initially possible given the basic structure of the machine. Therefore, additional components were modeled and 3D-printed in Solidworks to meet appropriate conditions for the test. Figure 16 below shows a simplified schematic of the test set up

where both ends of the vessel are fixed and a displacement is prescribed to the prototype.

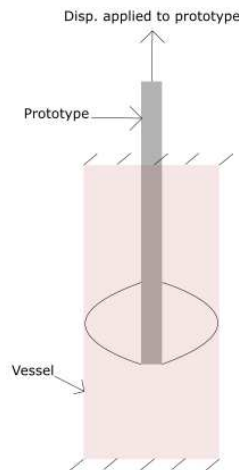


Figure 16: Simplified test set up of Experiment A. The hashed marks dictate that both ends of the vessel are fixed. An axial displacement is applied to the prototype using the LRX Plus Series Materials Testing Machine to allow the device to translate through the vessel and measure the force required during translation.

3.4.2: Experiment A with Dry PTFE

The designed component dictates that the bottom head of the machine fixes both ends of the tubing. The component was designed such that the bottom head can easily clamp it, and the PTFE tubing can fit inside the component such that the tubing cannot translate. The component has a hole cut out on top so that the wire of the prototype slips through. The wire of the prototype is then clamped by the top head, and the test then controls the translation of the prototype from within the tubing. Figure 17 below shows

how the 3D-printed component is used to fix the tubing, and Figure 18 shows how this 3D-printed component is incorporated into the test set-up.

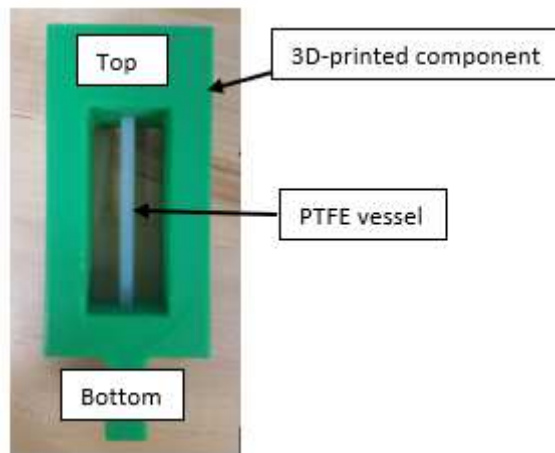


Figure 17: 3D-modeled component for fixing PTFE tubing in Experiment A.

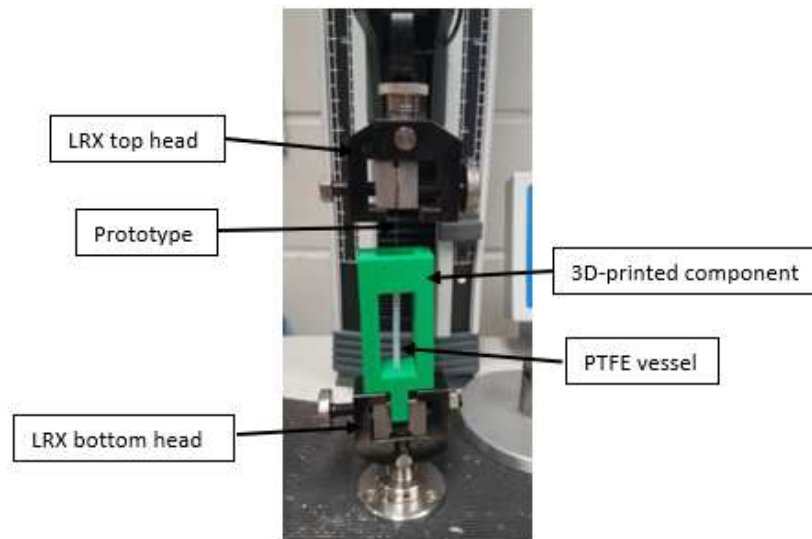


Figure 18: Experiment A test set-up with 3D-modeled component for fixing PTFE tubing.

Once the test 3D-printed component was secured within the bottom clamp, the PTFE tubing was placed within the component, fixing it in place. The tubing was then straightened as best as possible, and the prototype was placed into the tubing at a random axial location. The experiment was then designed in NEXYGEN. NEXYGEN has some basic test functions that are already imbedded in the software. One of these is the insertion/extraction test, and this is what was used in Experiment A. There are several options for this test. For every test in Experiment A, it was specified that the top head holding the prototype would move up at a rate of one-tenth of a millimeter per second for a total distance of one millimeter, and the resulting force over time is the output. The displacement of the top head, if the prototype is fixed, is the same as the displacement of the prototype. So, this specifies that the prototype also moved within the PTFE tubing at one-tenth of a millimeter per second for a total distance of one millimeter. A 100 Newton load cell was installed to the top head of the machine to apply the necessary forces. The location of the top head was zeroed along with its force output, and the test was initiated. The data gathered from this test was time, force, extension, and deflection. Time and force are explanatory, but extension is the height of the top head over time (considering the initial position), and deflection is the movement of the top head over time (disregarding the initial position). Ten trials of this test were performed, logging the data for each trial. The prototype was reset to its initial location after each trial.

3.4.3: Experiment A with PBS 1X-Hydrated PTFE

After Experiment A was conducted for dry PTFE tubing, the same experiment was performed using hydrated PTFE tubing. Before each of the ten trials, the tubing was hydrated with PBS 1X using a pipette. The PTFE tubing was removed from the 3D-printed component and ten drops of PBS 1X were applied to the inside of the tubing, rotating the tubing to assure the whole inner surface was coated. Once hydrated, the PTFE tubing was placed back into the 3D-printed component and the prototype was placed within the tubing and clamped to the top head. The NEXYGEN test was initiated for ten trials. It was crucial to perform this experiment on PBS 1X-hydrated PTFE tubing because the porcine artery was also hydrated with PBS 1X. This removes one confounder in this experiment and assures a similar testing environment between vessels, making the results and comparison between vessel types more believable.

3.4.4: Experiment A with PBS 1X-Hydrated Porcine Artery

After Experiment A was conducted for hydrated PTFE tubing, the same experiment was performed using the PBS 1X-hydrated porcine artery. The artery was difficult to work with. It dried out quickly and needed to be rehydrated often. Once it started to become dehydrated, it got sticky and was difficult to stretch and manipulate. It was also limp and slack, not holding the same rigidity as the PTFE tubing. As a result, there are some slight differences between this portion of the experiment and the previous ones. The artery could not be fixed at both ends like the PTFE tubing, and the

artery could not be clamped directly to the head of the machine because it needs to hold its diameter. If it were clamped directly to the machine, it would collapse and become narrow. A 3D component was modeled in Solidworks and printed to fix the artery to the bottom head while keeping its shape. The artery stretches over a conical profile to hold its shape, and the artery is then fastened to the cone with copper wire. The base of the component is then clamped to the bottom head of the machine. With the artery fixed at its bottom end, the wire of the prototype is then clamped by the top head, and the test again controls the translation of the prototype from within the vessel. This 3D-printed component is shown below in Figure 19, and the test set-up incorporating it is shown in Figure 20.



Figure 19: 3D-printed component for fixing porcine artery in Experiment A.

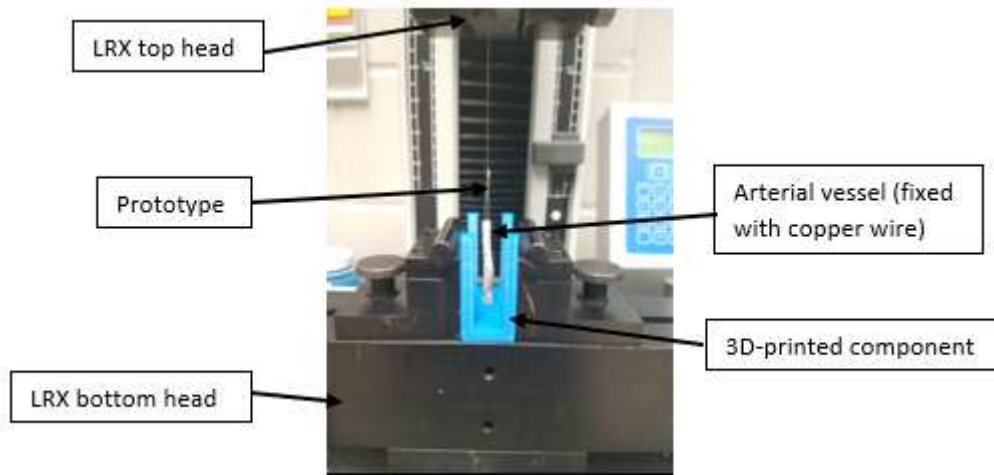


Figure 20: Experiment A test set-up with 3D-modeled component for fixing porcine artery.

When positioning the prototype within the vessel, sometimes the vessel needed to be held by hand to prevent bunching. The prototype did not insert entirely into the artery, but it was inserted enough so that the point of maximum distance between the spring profiles was contained within the artery, which should in theory give the highest slip force output. The artery was hydrated with ten drops of PBS 1X with a pipette before each trial. The NEXYGEN test was initiated for ten trials.

3.5: Experiment B – Artery in Tension

The porcine artery is not rigid like the PTFE tubing. It observably stretches when a force is applied to it. It is clear from Section 3.4.4 that the artery was not ideally constrained in Experiment A. It was potentially subject to axial displacement since it was not fixed at both ends. Because of this, it is desirable to examine the artery's behavior under axially load. This data can be used to explain the results of the artery slip force

test outlined in Experiment A. A simple tension test of the porcine artery was performed with the LRX Plus Series Materials Testing Machine. NEXYGEN has a tension test in its basic test library that applies a prescribed axial displacement to a material and measures the reactive force output throughout the test. Since this test takes the artery to failure by tearing it, it was only performed once. The artery was hydrated with PBS 1X using a pipette and then clamped to both heads of the machine, making sure it was taught. A 100 Newton load cell was secured to the top head of the machine to supply the necessary forces. Figure 21 below shows this test set-up on the LRX Plus Series Materials Testing Machine.

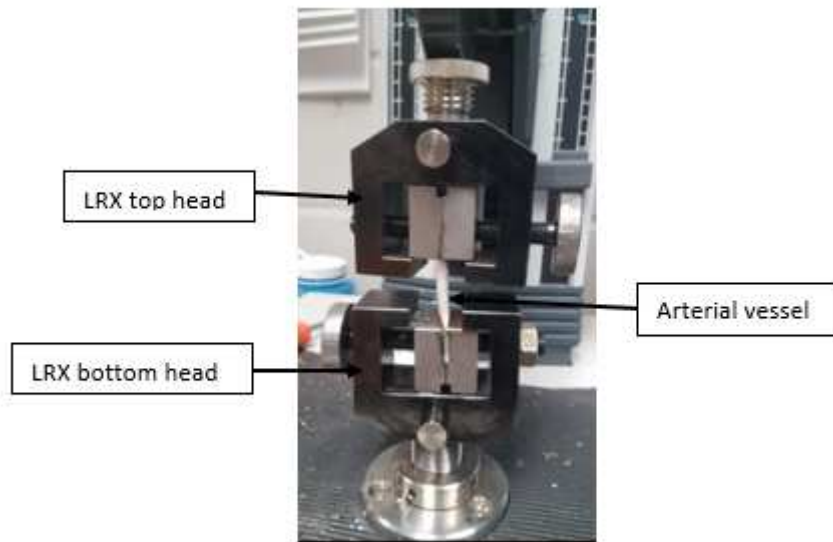


Figure 21: Experiment B set-up for tension test of porcine artery.

In NEXYGEN, the tension test was designed to move the top head at the same rate of one-tenth of a millimeter per second. However, instead of prescribing a total

displacement of one millimeter, a displacement of 100 millimeters was prescribed. This was drastically overshoot purposely to assure that the test would not terminate before the artery tore. The test was initiated via the lab computer and run until the artery tore completely.

3.6: Simulation A – Computer Simulated Slip Force Determination

After completion of Experiments A and B, Simulation A was conducted in Solidworks. The purpose of this simulation was to establish theoretical data for slip force, principle stress in the spring in the radial direction, and the spring constant of the spring. All these outputs were determined as a function of normal force applied to the vessel wall, radial displacement of the spring, and vessel inner diameter. These outputs all have their own importance. Slip force determination is critical for determining how the experimental slip force relates to the theoretical slip force given the vessel size used in Experiment A. This models the experiment to see if the prototype performs as it should. Principle stress in the spring is important because we want to know how the spring behaves in compression. If the stress in the spring reaches the flexural yield stress of the spring material, the spring will permanently deform, which denotes that the spring has failed. The spring constant is important because we want to see if the spring force is linear in relation to its displacement. Furthermore, Simulation A ultimately determines the applicability of this device for a range of vessel sizes, which is what a medical company or surgeon that uses this device in the future would want to know.

First, measurements were taken from Prototype C to model it in Solidworks.

Figure 22 below shows the measurements that were taken from the prototype to model the spring. The measurements were taken with micrometers (for dimension D) and calipers (for dimension L).

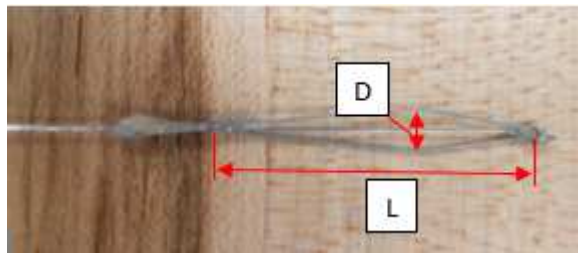


Figure 22: Prototype C measurements for Simulation A. $D = 0.1411$ inches and $L = 1.29$ inches where D is the maximum distance between springs and L is the length between fixed ends of the springs.

These measurements were then used to model one of the springs. There are a few important assumptions here. Remember that the number of springs would scale according to the application. Accordingly, only one spring was modeled with this simulation, and the prototype was assumed to be symmetric. This allows us to scale the number of springs easily since the spring force would increase linearly with the number of springs. This can safely be assumed because, for example, doubling the number of identical springs doubles the spring constant, which then doubles the spring force. Lastly, a tangent contact of 0.125 inches was assumed between the main wire and the spring at the springs ends. This is difficult to measure from the prototype. Figure 23

below shows the sketch profile of one spring given the prototype measurements and assumptions.

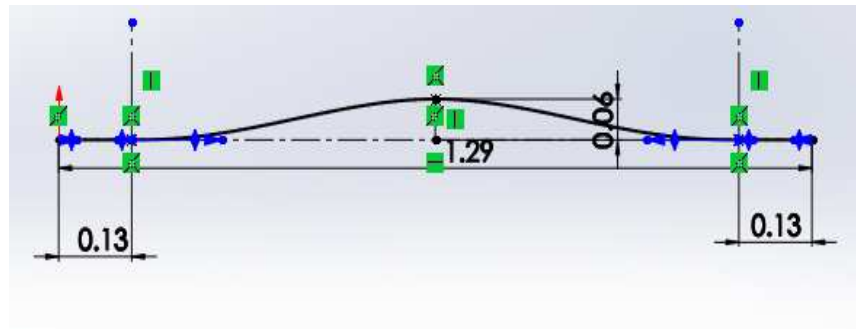


Figure 23: Simulation A spring profile. The precision shown on this sketch is one-hundredth of an inch, but the true values that have been specified on this sketch are accurate. The 0.06-inch dimension (true value 0.06055 inches) was calculated as follows: $(0.1411 - 0.01)/2 - 0.005 = 0.06055$ inches where D is 0.1411 in, 0.01 in is the diameter of the main wire, and 0.005 in is the radius of the spring. This was considered because Solidworks sweeps a path of the profile, so the center of the spring needs to be specified.

The profile of the spring was then swept to make it three-dimensional, and the spring was fixed at both ends. The initial radial distance from the central axis to the outside arch of the spring was noted. A point load was applied to the center of the spring to simulate spring force as a result of contact between the spring and the vessel.

Figure 24 below shows this simulation set-up.

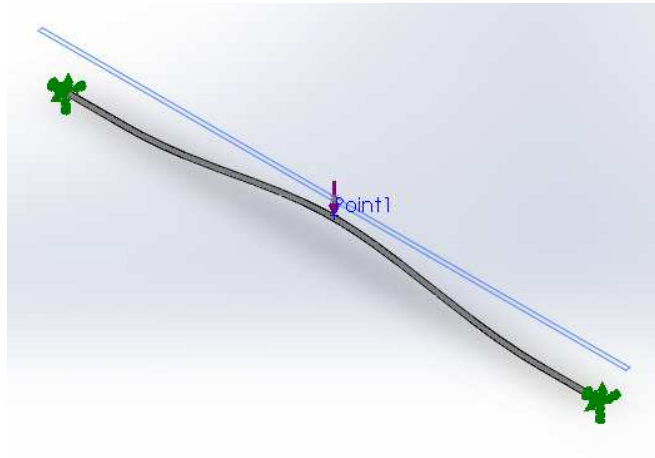


Figure 24: Simulation A set-up.

Prior to running the simulation, the material of the spring needed to be prescribed. While many titanium alloys exist in the Solidworks materials library, nitinol is not one of them. Properties of nitinol wire were researched, and the properties were input into a custom material in the library to most appropriately model the spring. Solidworks requires specification of the elastic modulus, Poisson's ratio, mass density, and yield strength to evaluate behavior of the material. The elastic modulus is 28 GPa, conservatively assuming low temperature ^[29]. Poisson's ratio is 0.3, mass density is 6.45 g/cm³, and the tensile yield strength is 100 MPa at low temperature ^[29].

The force was applied in increments of 0.05 Newtons from zero to 0.55 Newtons. Chapter 5, the discussion chapter, will explain why 0.55 Newtons was selected as the stopping point of the simulation. With each applied force, the principle stress in the radial direction of the spring was measured, as well as the radial displacement of the spring. The spring constant at each force was calculated by dividing the applied force by

the radial displacement. The applicable vessel diameter of each radial displacement derived from force applied was calculated using the following geometric equation:

$$X = (x_0 - d_r) * 2 + 0.254$$

Where X is the vessel diameter as a function of radial displacement of the spring, x_0 is the initial radial distance from the central axis to the outside arch of the spring (or point at which there is no radial displacement), d_r is the radial displacement of the spring, and 0.254 is the diameter of the main wire in millimeters. Finally, to model the prototype used in Experiment A, the number of springs in the device was scaled up to two. The slip force, or maximum friction force, was calculated for PTFE vessels and arterial vessels as a function of spring force and vessel inner diameter using the static coefficient of friction data previously stated ^{[8][14]}.

4: Results

This chapter is intended to show the results of the experiments and simulation explained in Chapter 3. The results shown throughout this chapter are both relationships between raw data and functions of the data that have been calculated. The results of the experiments and simulation are introduced in chronological order of when they were performed. Analysis of the data was conducted in RStudio for Experiments A and B, and MATLAB was used to analyze data for Simulation A. Displacement and diameter data were displayed in millimeters for easy comparison. Also, millimeters are typically used as the unit of measurement in the endovascular community.

4.1: Experiment A Results

The force curve was plotted for each of the ten trials for the PTFE vessel, the PTFE vessel hydrated with PBS 1X, and the porcine arterial vessel hydrated with PBS 1X. Additionally, to assure the prescribed displacement data corresponded to the force output, the displacement data for each trial of each vessel was plotted. The average curves for both force and displacement were calculated across trials for each of the vessels by averaging the data matrices at each time interval. More thoroughly, at each point in time of each data frame representing a trial, the force, extension, and deflection points were added and divided by ten to give the average data across trials. This averaging was performed for each point in time so that a matrix was formed that represented the average data across trials. Note that deflection is what NEXYGEN

software calls displacement. The term displacement will typically be used to describe deflection. Force and displacement outputs for Experiment A are shown below in Figures 25 through 30. These figures begin with the dry PTFE vessel, then the hydrated PTFE vessel, and finally the hydrated artery. Force curves are shown before displacement curves for each of the three scenarios. Each figure shows the output of ten trials (each trial is shown in blue) with the overlaying averaged curve (shown in red). Important points in the data have been labelled and described briefly in the figure captions where applicable.

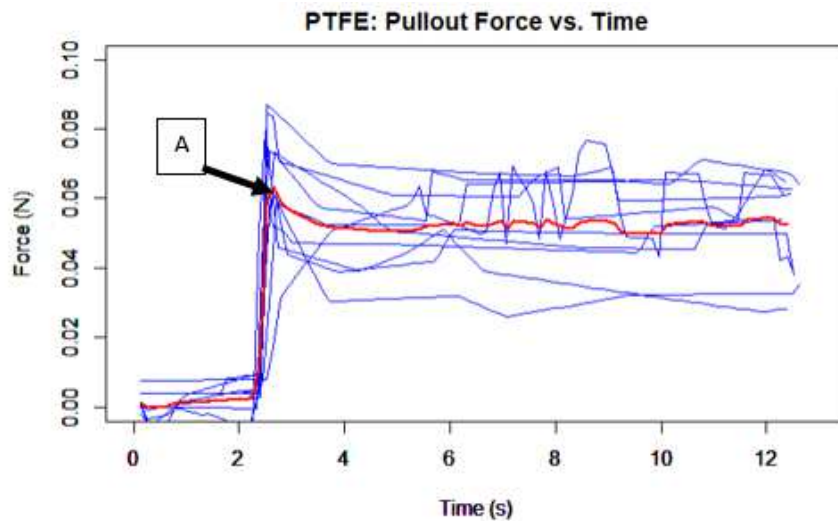


Figure 25: Experiment A force response – dry PTFE vessel for 10 trials. The blue lines represent the individual force output of each trial, and the red line represents the average force output of the ten trials. Point A denotes the peak force of the average curve, which dictates the force required for initiating displacement. Since this is the point at which the device starts to translate, this is also where the coefficient of friction goes from static to kinetic.

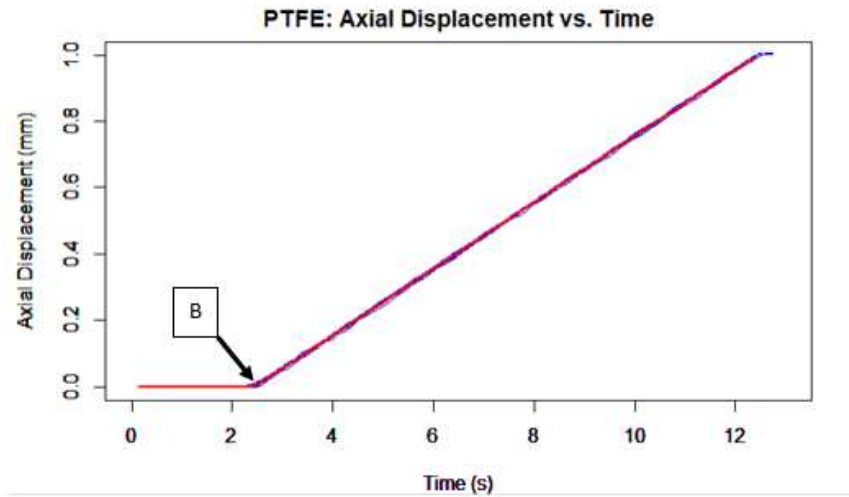


Figure 26: Experiment A displacement response – dry PTFE vessel for 10 trials. The blue lines represent the individual displacement output of each trial, and the red line represents the average displacement output of the ten trials. Notice that the displacement deviates from zero at point B in the average displacement curve, and this aligns with the time of peak force seen in Figure 25.

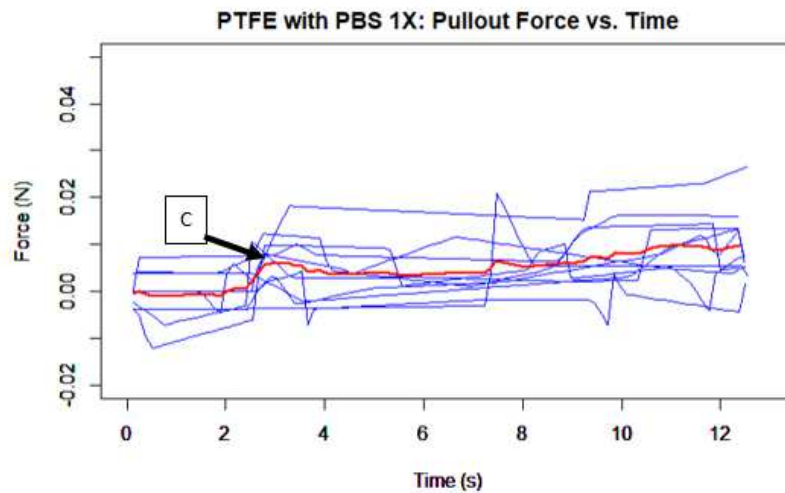


Figure 27: Experiment A force response – PTFE vessel hydrated with PBS 1X for 10 trials. The blue lines represent the individual force output of each trial, and the red line represents the average force output of the ten trials. While there appears to be no clear peak force like there is in Figure 25, point C on the average force curve dictates the force required for initiating displacement.

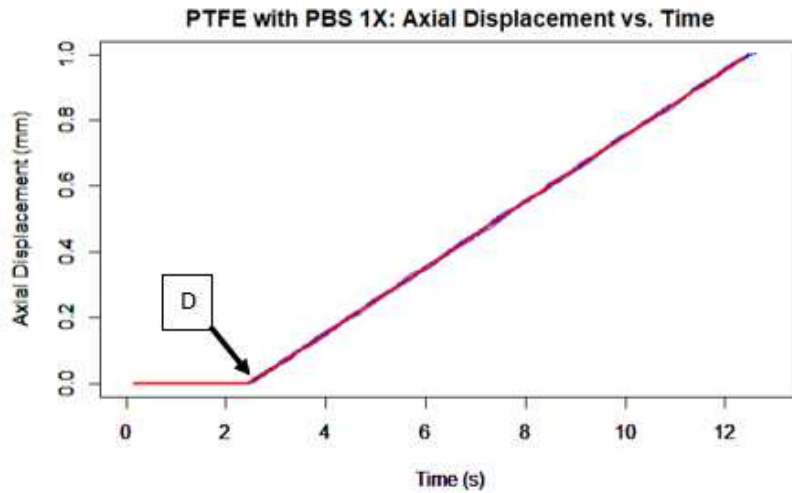


Figure 28: Experiment A displacement response – PTFE vessel hydrated with PBS 1X for 10 trials. The blue lines represent the individual displacement output of each trial, and the red line represents the average displacement output of the ten trials. Notice that the displacement deviates from zero at point D in the average displacement curve, and this aligns with the time of peak force seen in Figure 27.

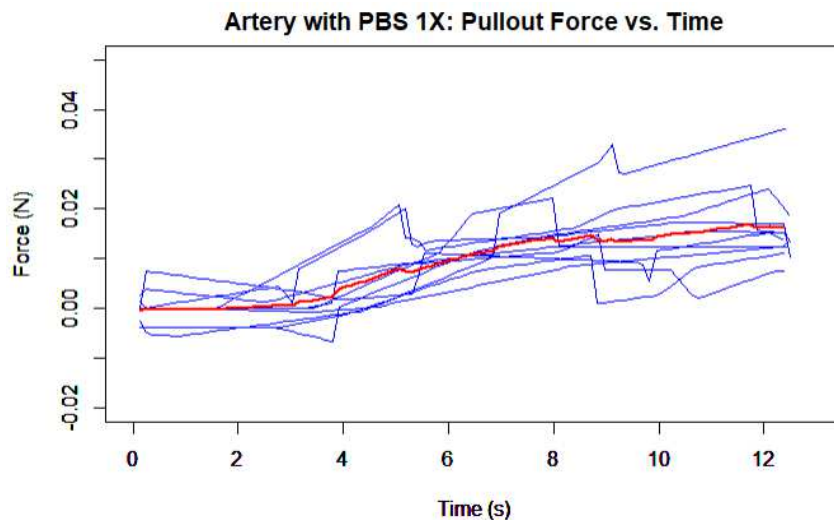


Figure 29: Experiment A force response – porcine artery hydrated with PBS 1X for 10 trials. The blue lines represent the individual force output of each trial, and the red line represents the average force output of the ten trials. There are no clear transition points in the average curve.

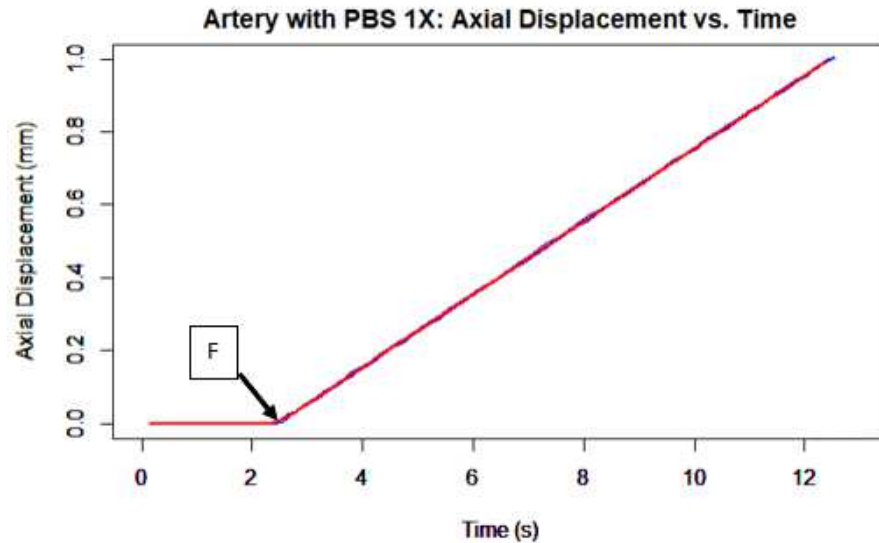


Figure 30: Experiment A displacement response – porcine artery hydrated with PBS 1X for 10 trials. The blue lines represent the individual displacement output of each trial, and the red line represents the average displacement output of the ten trials. Notice that the displacement deviates from zero at point F in the average displacement curve, but there is no true transition point to align this with in the force plot in Figure 29.

In continuation, the maximum force value was extracted from the data frame of each trial for each vessel. This allows us to generate a maximum force distribution for each vessel, which has been demonstrated in Figure 31 below using boxplots. Note that outliers on the upper end have been defined as points that are greater than the third quartile plus one-and-a-half times the inner quartile range, and outliers on the lower end have been defined as points that are less than the first quartile minus one-and-a-half times the inner quartile range. There are no low outliers, but there is one high outlier in the data.

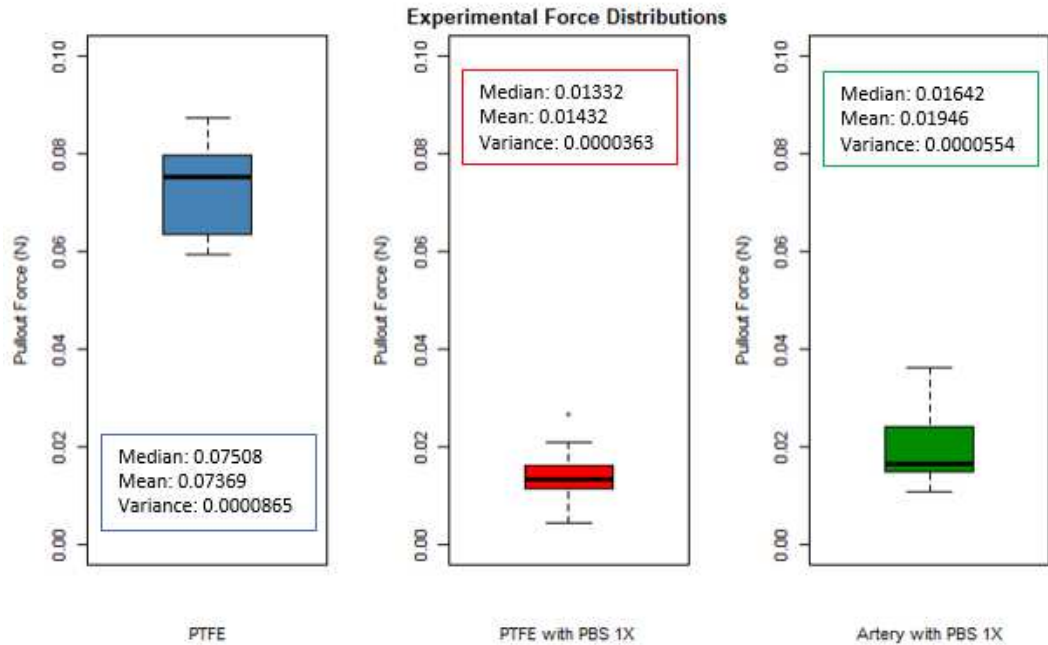


Figure 31: Experiment A - maximum force distributions.

4.2: Experiment B Results

The force curve was plotted for the porcine artery in tension as a function of deflection. As previously stated, only one trial was conducted for Experiment B since the experiment destroyed the sample. Using both the displacement input and the force response from the data, a spring constant was then calculated using Hooke's law. The spring constant was calculated for each time frame and plotted as a function of deflection throughout the test. The results of Experiment B are shown in the figures below. Figure 32 shows the force response of the porcine artery, and Figure 33 shows the calculated spring constant.

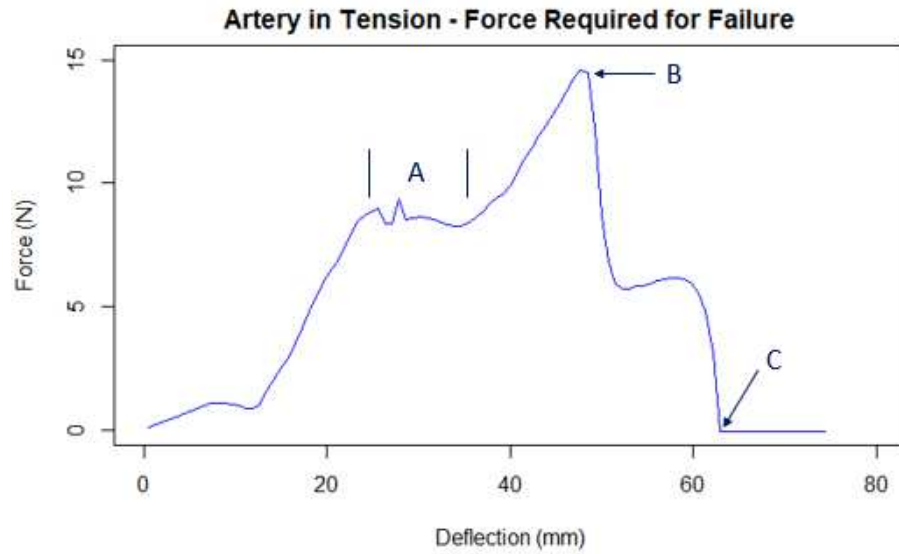


Figure 32: Experiment B - force response of porcine artery in tension. Section A shows the range at which the material exhibits yielding. Point B shows the maximum force output, or ultimate tensile strength of the artery. At point C, the artery has been completely severed.

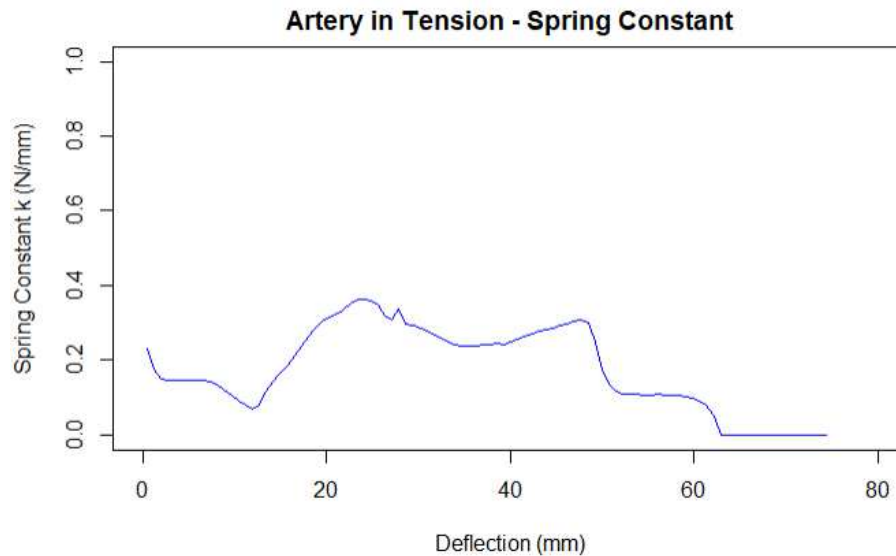


Figure 33: Experiment B - calculated spring constant of porcine artery in tension.

4.3: Simulation A Results

Once force and radial displacement data were gathered from the simulation, the spring constant was calculated as a function of these two variables using Hooke's law. The spring constant was calculated for each force input as a function of prescribed force, radial displacement, and vessel diameter, and plotted. The first two are straightforward. To examine how the spring constant relates to vessel diameter, the equation shown in Section 3.6 calculates the applicable vessel diameter for each radial displacement of the spring. x_0 in this equation was found to be 1.9190 millimeters by using the measuring tool in Solidworks. Now, by knowing x_0 , and by using the radial displacement d_r from the simulation, the spring constant can be calculated as it relates to vessel diameter. One important note here is that although this equation scales the device to two springs, the applicable vessel size is the same if there are any number of springs parallel about an axis. To avoid confusion, the visuals of the spring constant response to prescribed force, radial displacement, and applicable vessel inner diameter are the spring constant responses of only one spring.

Data for the principle stress in the radial direction of the spring was also gathered from Simulation A and is also plotted as a function of prescribed force, radial displacement, and applicable vessel inner diameter. Again, this stress response demonstrates the stress of one spring. The flexural yield strength of nitinol was researched and determined to be 870.9 MPa (assuming no esthetic coating of the

material) [1]. The stress response was plotted against the flexural yield strength to examine if the spring reaches failure. The highest stress value in the simulation is 608.2 MPa, assuring that the flexural yield strength was not surpassed.

Table 4 in Appendix A shows the raw data of prescribed radial force, radial displacement, applicable vessel inner diameter, resulting spring constant, and resulting principle stress in the radial direction. Figures 34 and 35 below show the spring constant response and principle stress response of the spring, respectively. Notice that open circles on the graphs indicate data points, and these data points are connected by a line.

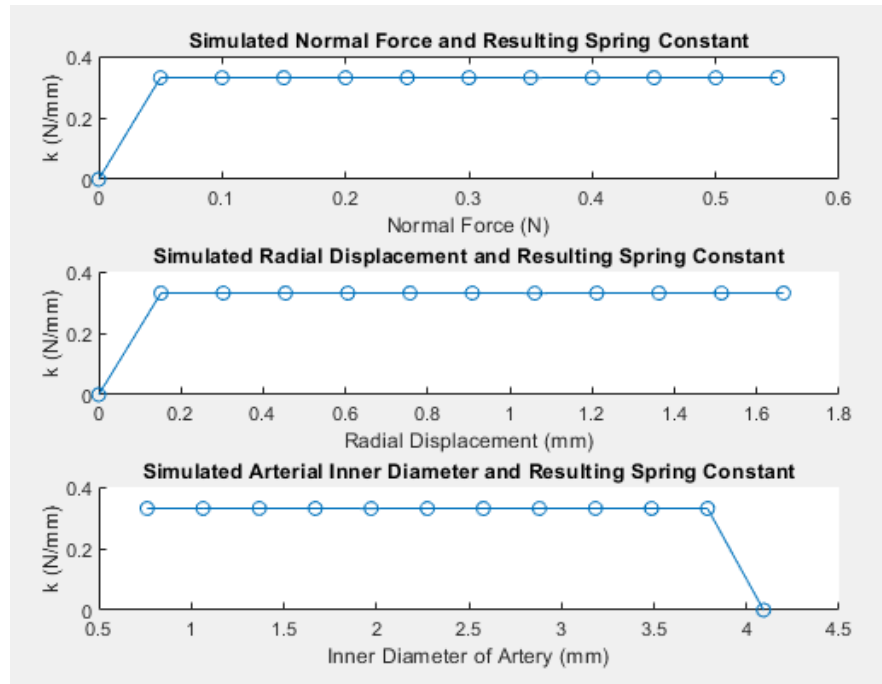


Figure 34: Simulation A - spring constant response.

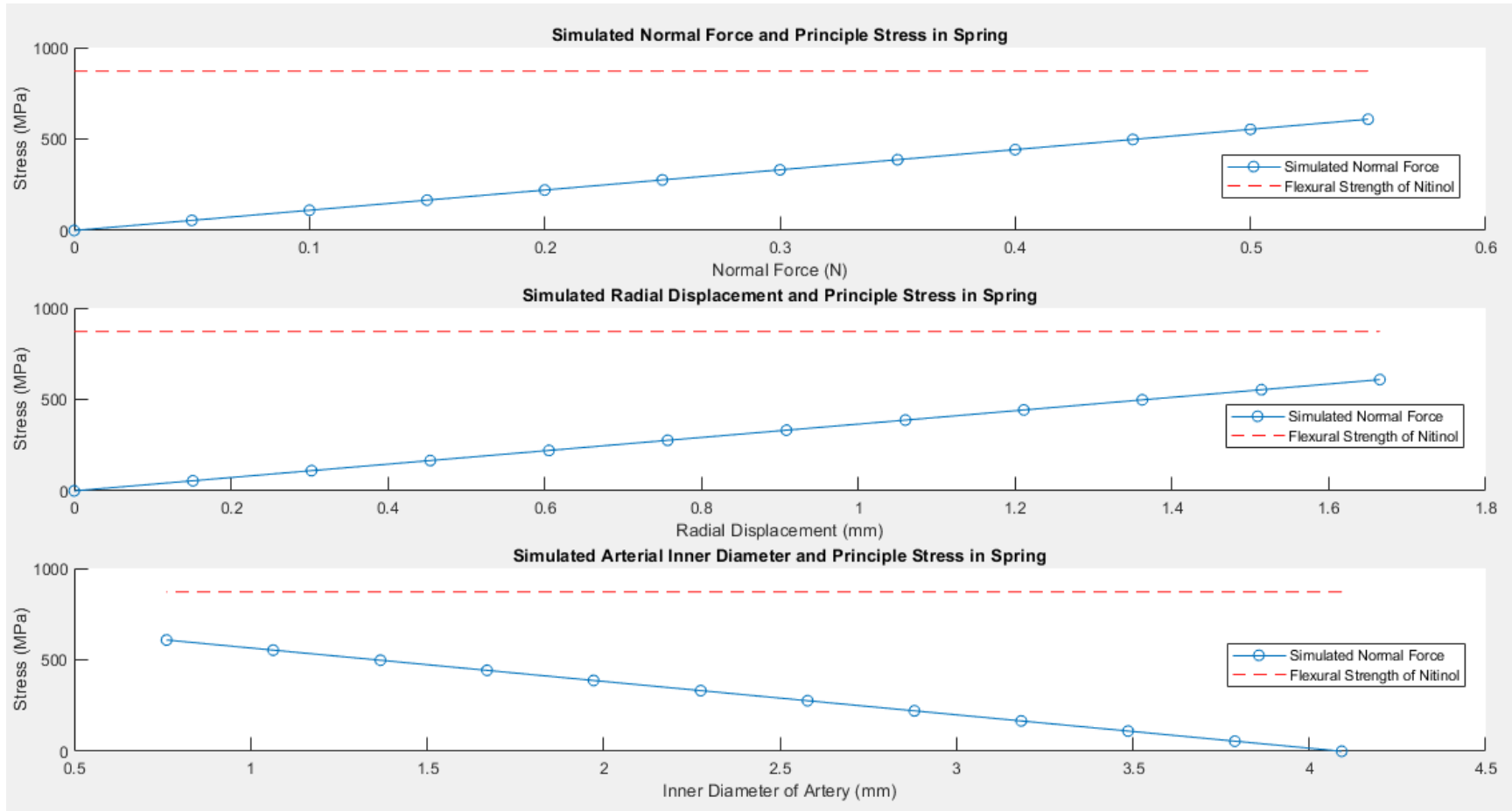


Figure 35: Simulation A - principle stress response in radial direction.

Next, the maximum friction force (also called pullout force and slip force throughout this paper) as functions of normal force to the vessel and vessel diameter were calculated for both PTFE and arterial vessels. This is a major component of this research because it shows the theoretical application of the device. Before calculating the maximum friction force however, the data was scaled to a device of two springs. This means that the prescribed force data in Table 4 was doubled to simulate the normal force that would be applied to the vessel. The maximum friction force was calculated from the normal force by using the static coefficients of 0.1 for the artery and 0.06 for PTFE [8][14]. The friction force as a function of normal force, as well as the friction force as a function of vessel diameter, is plotted in Figure 36 below for a two-spring device.

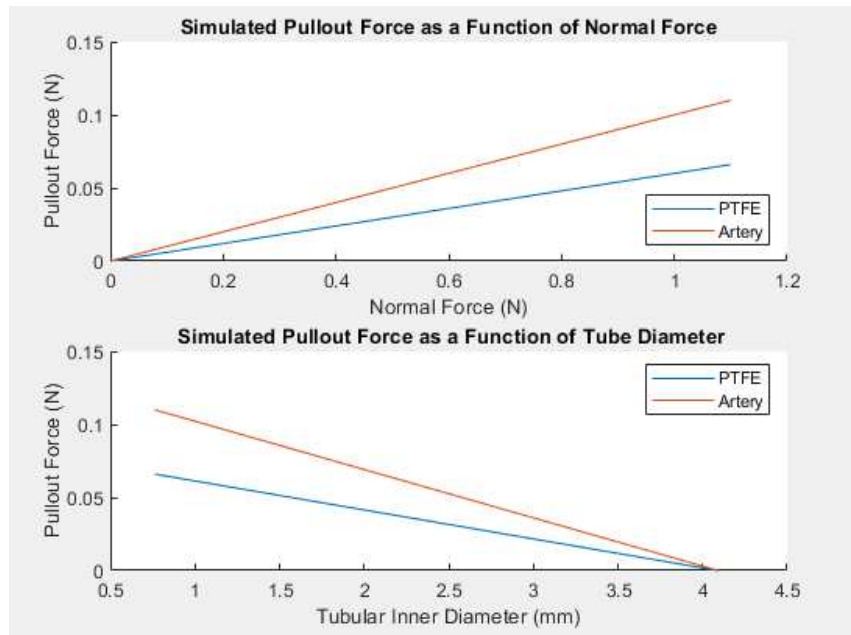


Figure 36: Simulation A - pullout force for a two-spring device.

Finally, now that the pullout force was determined as a function of vessel size, the simulated results were compared to the experimental results. The pullout force for both the PTFE and arterial vessels were calculated using the data in Table 4 for the corresponding vessel sizes. Linear interpolation was necessary here because the vessel inner diameters are 4 millimeters for the artery and 3.175 millimeters for the PTFE, neither of which are data points for applicable vessel inner diameter in Table 4. It was crucial to again double the prescribed force values when calculating the theoretical pullout force because the prototype has two springs. The theoretical pullout force within the PTFE vessel was calculated to be 0.0182 Newtons, and in the porcine artery, it was 0.003 Newtons. These values were overlaid on Figure 31 to compare the simulated results to the experimental pullout force distributions. This is shown below in Figure 37.

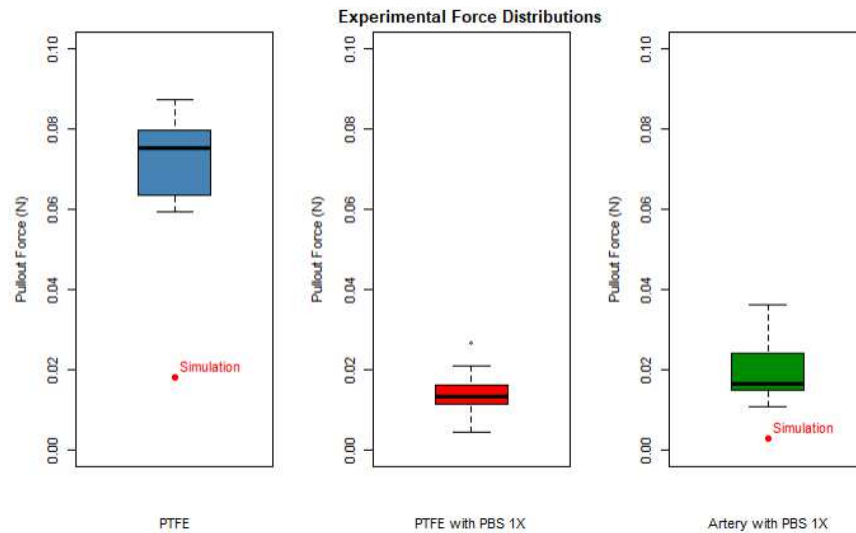


Figure 37: Pullout force comparison between Experiment A and Simulation A.

5: Discussion

This chapter will discuss the overall interpretation of this work from start to finish. First, the effectiveness of the prototype and its comparison to a finalized device will be addressed. Next, the results of the experiments will be discussed, followed by the results of the simulation. The goal of this chapter is to explain the data, provide reasoning for unexpected data, and suggest techniques to improve the accuracy of the results if this work were to be performed again from the beginning. Suggestions for future work based on results of this research are discussed in Chapter 6.

5.1: Prototype C Construction and Effectiveness

Prototype C was a crude approximation of a finalized design. Overall, it was able to achieve the goal of applying a radial force to the vessel to prevent, at least to some degree, the device from slipping out from the vessel. The nitinol material held up well throughout experimentation, and no permanent deformation was noticed. The prototype brings with it some obvious shortcomings though. First, it used super glue to hold the springs to the main wire. Ideally, these would be manufacturing processes. The cleanest prototype would be one in which the springs are micro-soldered to the main wire. Referring to Figure 14, micro-soldering would clean up the adhesion points. As previously stated in Chapter 3, micro-soldering of nitinol to nitinol is possible with gold tin or tin silver. While it is likely an expensive process, typically we are not concerned with cost in a medical context if the device performs the appropriate function. It is

unclear how much this process would cost, but it is suspected to be acceptable. Next, the springs were pre-shaped by hand. This is not ideal because there is no way to assure identity of the springs, which is desirable so that the device is symmetric. If the device is symmetric, it applies the same force to the vessel at both contact points given a fixed vessel size. Identical springs make it easier to scale the device for the application as well. The device should utilize shape-set springs that can be manufactured to a specific curvature, which assures identical springs. Finally, the springs may not be aligned exactly 180 degrees from each other. Without radial symmetry of the contact points, the “settling point” of the main wire might be pushed away from the center of the vessel. Thus, it would be ideal to align the springs with the appropriate offset.

It is possible that the shortcomings of the prototype influenced the results of Experiment A. While this likely has a minimal effect on the results, the springs likely did not apply identical forces to the vessel wall since their curvatures were not identical. If the springs were identical, the force outputs of Experiment A may have been slightly greater. If the springs were matched to the spring with the greater radial arch, then the spring that was scaled up in radial curvature would generate more force since it then compresses more. This would lead to a greater slip force output.

5.2: Experiment A - Interpretation of Results

This section will discuss the results of Experiment A. The first subsection compares the peak force values among the various vessels in the experiment. The

following three subsections examine the force and displacement curves of the device within the three vessels in detail, as well as the force distributions of each. The results of each model will be explained individually and will include discussions on variations in the data as well as how the data compares to expectations. Also included in the following subsections are suggestions on how Experiment A could have been designed differently to assure accurate results for each vessel, and how the force output can be increased while still considering biological constraints.

5.2.1: Comparison among Peak Forces for Various Vessels

The median friction force within the dry PTFE vessel was just shy of 0.08 Newtons. Within the hydrated PTFE vessel and the hydrated artery, the median friction forces were both just shy of 0.02 Newtons, with the artery holding a slightly higher median. The force distributions of the hydrated PTFE and the hydrated artery are quite similar, and this is likely because they were hydrated with the same medium. This dictates that PTFE hydrated with PBS 1X is a sound model to demonstrate the force output of the device in an isolated porcine artery hydrated with PBS 1X, which shows that the decision to use PTFE as a model is justified. While these median friction forces in the hydrated PTFE and arterial vessels seem low, it is unclear how much friction force the device needs to generate to restrict stent-anchoring wire advancement and oppose the unsheathing force of the microcatheter. To the author's knowledge, there are no established guidelines that detail the force generated by the stent-anchoring wire upon

unsheathing the stent nor the force at which the microcatheter is retrieved to unsheathe the stent (i.e. the force applied by the surgeon). The inner quartile range of the three portions of this test appear repeatable. That is, the inner quartile range is not large relative to the data sets. Perhaps more trials could have been performed in this experiment to demonstrate the repeatability.

Remember that the device can be scaled to include more springs to increase the friction force. Although, there reaches a point where the device would occlude the artery *in vivo*, so we can only add a finite number of springs. If this device were to be used *in vivo*, appropriate blood flow must be maintained throughout the artery. To the author's knowledge, there are no established guidelines for blood flow reduction due to catheterization that negatively impacts the patient. This introduces a major future direction of this work that will be discussed further in Chapter 6. Another method to improve the friction force is to increase the spring force. This means that the spring curvature needs to be increased so that it compresses more in the vessel, or the stiffness of the spring needs to be increased. The only efficient way to change the spring constant is to change the spring material or make it thicker. However, nitinol is a great material for this application since it is already used in the endovascular space, and it can be shape set. So, the most appropriate action would be to increase the spring curvature. Since the inner quartile ranges are somewhat large, especially in the porcine artery, more trials

would likely introduce more outliers to the data and increase the inner quartile ranges if the evaluated trends continue.

5.2.2: Dry PTFE Vessel – Force and Displacement Curves

The average force curve for dry PTFE tubing (refer to Figure 25) is what we expect from this experiment. We expect that the device will slip from the vessel with some force that relates to the static coefficient of friction (μ_s). This is the peak force represented by point A in Figure 25. The device then continues to translate through the vessel after initial slip at a force that relates to the kinetic (μ_k). The kinetic coefficient of friction is lower than the static coefficient of friction, which explains why the force output reaches a peak force and then stabilizes at a lower force. Also, comparing Figure 25 and Figure 26, we see that the displacement curves match the force curves. That is, the peak force output aligns to the same moment in time ($t = 2.5s$) in which the device displaces from its initial position. This verifies that the test was run properly. The displacement data for each trial matches almost exactly, so the test was repeatable across trials.

However, the variation of force output across trials for the dry PTFE vessel cannot go unnoticed. While the scale on the force axis is small, there is still a difference in force of about 0.04 Newtons between the lowest and highest stabilization forces. Nine of the ten trials hold the same curve shape where they reach a peak and then stabilizes at a lower value. One of these trials though does not reach a peak at the same time as the

others, and it does not seem to stabilize. There are large fluctuations in force throughout this trial. This trial could be considered an outlier since it does not match the performance across other trials, but it should still be explained. The fluctuations could be a result of user error. For example, I may not have reset the location of the device appropriately before this trial, and the device could have found a small bend in the PTFE vessel. The PTFE vessel was straightened as best as possible just by visualization, but it was not perfect. If the device found a bend in the vessel, it may have required more force to pull through, and it may not have had the opportunity to stabilize if the path was changing. Furthermore, the load resolution of the LRX Materials Testing Machine is less than 0.005 percent of the load cell used ^[22]. While this is extremely sensitive, a 100 Newton load cell was used, which means the maximum error in force output across both Experiment A and Experiment B is 0.005 Newtons. Since the magnitudes of force in Experiment A are in the range of tenths of a Newton, the machine sensitivity can contribute to some of the fluctuations throughout each trial and the variance across trials.

To limit the possibility of reducible error, the vessel should have been straightened appropriately. Although I have not tried this, there is a crude trick that is used to straighten plastic tubing. Apparently, the tubing can be heated in boiling water for a few minutes to soften it, which allows it to be shaped into a straight line. However, arteries are not straight, so this suggestion just addresses the effectiveness of Experiment

A. A symmetric device with identical springs would give the device the best performance shall it be used in vivo so that each spring applies an equivalent force to the vessel wall at any point in the vasculature.

5.2.3: PTFE Vessel Hydrated with PBS 1X - Force and Displacement Curves

The average force output (refer to Figure 27) is a bit troubling here. The curve seems to reach a small initial peak once the device has slipped from its initial position within the vessel, but it does not stabilize at a lower force like we would expect. Instead, the force output continues to climb throughout the remainder of the test after a very brief stabilization. Perhaps this experiment should have been taken to a further displacement to see if the force ever stabilized. For example, if the device moved at a prescribed displacement of five millimeters instead of one millimeter, maybe a stabilization force corresponding to the kinetic coefficient of friction would be clearer. This could explain why the peak force of most of the trials typically occurs at the end of the time period. Thus, when comparing the peak force among the various vessels, it is important to remember that the peak forces do not occur at the same points in time.

Nonetheless, the displacement curves match the force curves (refer to Figures 27 and 28). The first initial peak force corresponds to the point in time of the first displacement of the device, verifying a proper repeatable test. Some of the force values across all trials are puzzling. For example, there are several trials in which the force output drops below zero. The machine used in the experiment was calibrated to an

initial force output of zero. Since the vessel was hydrated, we expect the force outputs to be lower than those of the dry PTFE vessel. In this experiment, it is possible that since the device initiated a minimal friction force to the vessel, what is essentially shown in the data at negative forces is noise that can be attributed to the resolution on the LRX Materials Testing Machine. This portion of the experiment should have been repeated to reduce some of the uncertainties in the results. The test was set up properly, and the components were fixed in such a way that the boundary conditions should not have affected the data. The device should be scaled with additional springs, or the device should be tested in a smaller vessel. This would potentially eliminate some of the fluctuations in the data since the friction force output would be higher. While the fluctuations in the data are visually unappealing, the difference in force output between the minimum and maximum force output is only about 0.03 Newtons. So, if the peak force output could be scaled up to expect a peak of say 0.1 Newtons, these fluctuations would appear minimal.

5.2.4: Porcine Artery Hydrated with PBS 1X - Force and Displacement Curves

The average force output is like that of the hydrated PTFE tubing where the force output continues to climb throughout the test (refer to Figure 29). One distinct difference between the two though is that a clear initial peak is not reached in the porcine artery. A likely reason for this is that the boundary conditions for the porcine artery portion of this experiment were not ideal. Since only the bottom end of the artery was fixed to the

3D-printed component (refer to Figure 20 in Chapter 3), this left the top of the artery to move freely, so the body was not a true fixed vessel. Likewise, the artery did not hold rigid like the PTFE vessel, so when the device was withdrawn from within the artery, it is likely that these force results are capturing both the friction force of the device and the force it takes to stretch the artery. Thus, Experiment B was performed to characterize this phenomenon. The magnitude of the mean maximum force is relatively low at 0.01946 Newtons, especially compared to the mean maximum force of the dry PTFE vessel at 0.07369 Newtons. Recall though that the inner diameter of the artery is larger than that of the PTFE vessel, so the springs do not compress as much in the artery. This means the friction force would be lower in the artery, which is shown in the results. Again, there are fluctuations among trials, but it appears that the trials, at least most of them, hold the same relative shape. While the force outputs are non-uniform, notice the scale of the axis. The difference between the maximum and minimum peak forces is only about 0.02 Newtons, so these fluctuations could hopefully be cleaned up if the test was run more appropriately.

Ideally, this portion of the experiment should have been taken to a further displacement to see if the force ever reaches a peak. It would have been ideal to run the test until the device withdrew completely from the vessel, but given the boundary conditions of the test, this was difficult to do. The artery would have reached a maximum stretch at the end of this test, and since the artery was fixed to the 3D-printed

component only with copper wire, I would not have expected it to hold its place.

Furthermore, if the artery stretches throughout the test, the results would be skewed anyway, so the one-millimeter displacement was maintained for homogeneity throughout the experiment. Looking at Figure 30, we still see that the displacement is accurate.

This test was not an accurate depiction of the device's performance *in vivo*. The goal of this test was to establish an initial guideline to examine how the device achieves its purpose of applying a force to the artery. There are many other considerations that were not addressed in this test. For example, the artery would be more rigid *in vivo*. When the artery is subject to pressure from blood flow, it becomes more rigid. Think of the analogy of a garden hose. Although the scale is much larger, the hose initially appears limp and flexible, but when pressurized with water, it gets stiffer and more rigid. We would expect this phenomenon to some degree *in vivo*, which would exclude the consideration of large deflection of the artery. Also, for this experiment to be ideal, blood flow should have been supplied, which introduces yet another force that the device must overcome.

5.3: Experiment B - Interpretation of Results

This experiment was straightforward, so it is not necessary to go into as much detail as Experiment A. Again, this experiment was used to demonstrate the mechanical behavior of the porcine artery under axial tension. As seen in Figure 32, the force

required to extend the artery starts to climb immediately. This means that the test was set up properly where the artery was initially taught. Perhaps the artery could have been stretched initially so that it was under minimal load. There is one portion of the force output curve in which the force deviates from the curve. This is at a deflection of about 25 millimeters. This happened because I could see the artery start to slip from the top clamp, meaning it was not tightened enough. I tightened the clamp while the test was still running, so the test also measures the force that I applied. This can be disregarded from the force output as it was human error. The artery showed clear necking before rupture as shown below in Figure 38.

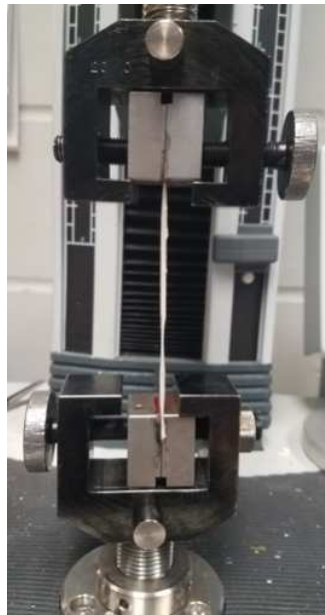


Figure 38: Experiment B - necking of porcine artery.

Referring to the force response of the artery under axial tension in Figure 32, the curve follows the general shape of a stress-strain curve until peak load denoted by point B. Section A on the curve shows clear yielding behavior where the vessel starts to deform permanently. The section of the curve between the yielding region A and the peak load B demonstrates strain stiffening, which biological cells tend to do when their cytoskeletal protein filaments align ^[17].

After the peak load of about 14 or 15 Newtons is experienced, the vessel begins to strain soften and necking occurs. Here, the vessel has begun to tear, but some fibers are still intact, leading to the necking behavior seen in Figure 38. The artery is not completely severed until the force output is zero, which is shown as point C in Figure 32. Once the force got to zero, the test was run for additional time to assure the force output remained zero.

The spring constant shown in Figure 33 has a nonlinear behavior which is expected for biological tissue. Overall, since the artery deflects when a force is applied to it, even in low ranges, this explains the fact that the device did not reach a true peak friction force within the artery in Experiment A. Since the artery was not fixed and the artery has a spring constant even at low forces, Experiment A was likely capturing the reaction force of the artery under the specified the prescribed displacement. Experiment B was more of a characteristic experiment in that the behavior of the artery under load was more crucial to examine than data points of interest, like the peak force value and

the spring constant at peak force for example. The only suggestion to improve this experiment is that the artery should have been tightened more carefully before the test so that I did not have to fix this during the test, which altered the data in one small range.

5.4: Simulation A - Interpretation of Results

This subsection will discuss the results of Simulation A. Before getting into the interpretation of the results, it is a good idea to discuss the simulation itself, including the simplifications it assumes. The first subsection will explain the believability of the simulation and the differences between the simulation and prototype. Next, the results of the simulation will be interpreted, including the friction force output for the different vessel types. Lastly, the results of the simulation will be compared to the force distributions of Experiment A, and a discussion will follow to explain the differences.

5.4.1: Accuracy of the Simulation

As discussed in Chapter 3, the simulation assumes a spring shape in which the ends of the spring are tangent to the main wire, the radial arch is symmetric, and the springs are aligned 180 degrees apart. While this is ideally how the device would be designed, it is likely not an accurate depiction of the prototype due to human error in prototype construction. In continuation, this simulation assumes a point load, which is not entirely applicable to the function of the device either. At first, I enclosed the modeled device into a vessel and tried to prescribe a radial displacement of the vessel to

give an accurate deformation of the spring. As the spring deforms more (that is, the device is placed into a narrower vessel), we would expect multiple contact points between the spring and the vessel. This also would have allowed us to determine the radial stress on the vessel due to spring force as well, which is another consideration that should ideally be accounted for. I chose to make the simplifications that I did in Simulation A to assume a point load, which means that the vessel and spring only have one point of contact. While this may not be perfect, it should give an educated estimate as to the theoretical performance of the device under these conditions. The boundary conditions of the simulation were sound. The ends of the spring were fixed, which is what would happen in theory when the springs are micro-soldered to the main wire or an adhesive is used.

5.4.2: Data Discussion

Notice in Table 4 in Appendix A that the maximum radial force that was prescribed to the spring was 0.55 Newtons. There is an important reason that this maximum was set. At 0.55 Newtons of prescribed radial force, the applicable vessel diameter is 0.7619 millimeters. Since the components of the device are three 0.254-millimeter (or 0.01-inch) wires, the space that is occupied by the device itself is 0.762 millimeters. This means that the device cannot fit into a vessel that is smaller than the size of the components, and 0.55 Newtons is the radial force at which the applicable

vessel inner diameter is the size of the components (- 0.0001 millimeters, which is certainly close enough for this purpose).

The spring constant data depicted in Figure 34 is expected. The spring constant is linear throughout the range of prescribed forces. It appears from the graph that the spring constant is increasing between a prescribed force of 0 and 0.05 Newtons. However, this is not really the case due to the sample size and the fact that the spring constant was first calculated at zero. If we took a force between zero and 0.05, I expect that the spring constant would be 0.33 Newtons per millimeter to match the performance elsewhere in the simulation.

The principle stress in the spring (refer to Figure 35) is also not surprising since the data matches the trends that are expected. As more force is applied to the spring, the stress in the spring will increase. Accordingly, as the inner diameter of the vessel decreases, the force placed on the spring increases, which is why the stress in the spring and vessel size have an inverted relationship. The linearity of the principle stress in the spring is favorable. This shows that the spring is only deforming elastically at these prescribed forces, so there is no permanent deformation. This is verified by the fact that the principle stress never reaches the flexural strength of nitinol. Thus, this is proof that the device will not fail during a procedure. Since the flexural yield strength is 870.9 MPa and the simulated maximum principle stress is 608.2 MPa, dividing the former by the latter gives a factor of safety is 1.432.

The slip force is linear for both the arterial and PTFE vessels. This is expected because the slip force was calculated as a function of normal force and the static coefficient of friction. The former scales according to the prescribed spring force, and the latter varies depending on the vessel type. Furthermore, the slip force within the artery is always higher than that of the PTFE tubing because the coefficient of friction of the artery is greater. Figure 37 shows that the simulated slip force values corresponding to the experimental vessel sizes are 0.0182 Newtons for dry PTFE, and 0.003 Newtons for the PBS 1X hydrated porcine artery. For reference, Table 2 below shows how these simulated maximum friction force values compare to the mean maximum friction forces determined in Experiment A. Note that a simulated slip force was not calculated for PBS 1X hydrated PTFE because I could not find a definitive static coefficient of friction matching this situation in published literature. The simulated slip force is closer to the experimental results for the artery than it is for dry PTFE.

Table 2: Comparison of experimental and simulated maximum friction forces

Vessel type	Experimental mean maximum friction force (N)	Simulated maximum friction force (N)
Dry PTFE	0.07369	0.0182
PTFE hydrated with PBS 1X	0.01432	-
Porcine artery hydrated with PBS 1X	0.01946	0.003

These differences between experimental and simulated slip force are likely due to the simplifications of the simulation. As discussed earlier, when the springs deform to fit within the vessel, the area of contact that is not well modeled by a point load. This contact would require that the spring deforms in a nonlinear fashion, and each small displacement within the spring initiates a portion of the overall normal force to the vessel. If this could somehow be modeled in a simulation, the slip force calculated from the simulation data would almost certainly increase.

6: Conclusions

This chapter will first summarize the overall performance of the device, stating both its strengths and weaknesses. Next, the chapter will provide a discussion on necessary future work stemming from this research to bring this device into use in endovascular neurosurgery. This includes further *ex vivo* experimentation that accounts for more variables to simulate an *in vivo* environment, filing intellectual property, animal testing, FDA approval, and clinical trials. Finally, the chapter will end with the value of this research will be addressed.

6.1: Summarization of Device Performance

This work demonstrates the initial development of a medical device from the beginning. A critical problem in endovascular neurosurgery was identified, a novel device was designed to address that problem, and then the initial stage of testing the effectiveness of the device was conducted. Experiment A shows that the device can generate the appropriate shape of the force curves that are expected by this device, at least for a dry PTFE vessel, and this is a success. This work shows that PTFE is a relatively accurate model for a fixed artery *ex vivo*, and this principle can be utilized in future scientific work.

Even though the friction forces initiated by the device seem low, to the author's knowledge, there are no established guidelines on the forces induced in flow-diverting stent delivery. Accordingly, it is unclear whether the forces initiated by the device are

physiologically relevant to have an impact on the procedure. The previous chapter explained some reasoning for the force magnitudes generated by the device, but since the ideal forces are unknown to the author, it is not fair to conclude the experimental and simulated results are not ideal. The prototype could have been made with more of a technical and accurate approach, the experiment that evaluated the performance of the device could have considered other variables, and the simulation likely did not render a true depiction of the device. The device may need scaling and design iterations to achieve appropriate force curves for vessels that more closely match an *in vivo* environment. Also, it is important in medical device design to establish a guideline for the optimal performance of the device, which is why the simulation needs further development. Furthermore, experimentation needs to be designed to dictate as many biological considerations as possible to truly evaluate the device's capabilities *in vivo*.

6.2: Future Work

First, an invention disclosure form will be filed through the Duke Office of Licensing and Ventures, and a provisional patent will be filed too. Even though the device needs to be scaled according to the required force, this is a unique feature of the design itself, so this will be included in the patent. There is minimal data on the forces that exist in intracranial stent placement, so it would be worthwhile to establish a guideline for how much force the device needs to support to scale the device properly. It is unclear how such a study would be performed. Perhaps a study within the

catheterization lab at a healthcare system can ask neurosurgeons to match the forces they impose when unsheathing a stent to a force gauge, or somehow fix a force gauge to the stent delivery system to measure the force of the surgeon's hand. Nonetheless, this still does not capture the force that sends the stent-anchoring wire forward, so this is another consideration that needs to be calculated in the future.

Further testing of device performance is required. First, it is important that the prototype is constructed more accurately. That is, the radial arches of the springs should match so that the device is symmetric. This would allow for optimal performance, and the simulation would better depict the prototype. This work could be outsourced to a medical device company or materials processing plant after intellectual property is filed. Once a more accurate prototype is made, Experiment A should be performed within an arterial vessel with a more realistic biological scenario. For example, if blood flow could be simulated, this provides an additional force consideration that would give us a better idea of the force output required by the device. Also, if this device were to be used *in vivo*, appropriate blood flow must be maintained throughout the artery. To the author's knowledge, there are no established guidelines on how much blood flow is necessary to allow brain function to be uncompromised, but this introduces a major consideration of this work. Since the device cannot occlude the artery, there will be a trade-off between the number of springs and blood flow. This relationship needs to be established as well as the blood flow required through an intracranial artery to assure patient safety.

Iterations should be made on the new prototype until an optimal force curve is achieved. This may include altering the radial curvature of the springs and scaling the number of springs so that the maximum force is achieved without tearing or perforating the artery. The simulation should also be altered to allow calculation of radial stress within the vessel since this is a critical consideration that these studies ignored. Also, the simulation should be readdressed to mimic a more realistic loading condition of the spring, which was a limitation with the point load application.

Once bench-top testing validates that the device can initiate appropriate forces to the vessel wall, the next possibility is animal testing. It might be possible to conduct this study in the Vivarium at Duke with domestic pigs since their circulatory system is like that of humans. Obviously, it is not possible to measure the friction force supplied by the device using an apparatus like the LRX Plus Materials Testing Machine, so this animal study would likely be designed to visualize device performance with angioplasty. Since the purpose of the device is to oppose both stent-anchoring wire and microcatheter forces, perhaps in an animal study, a surgeon can utilize the device while observers determine if the device stabilizes the stent delivery system with an angiogram. It would also be wise to gain insight from a surgeon on the convenience of the device. Ultimately, the device should be simple enough for the surgeon to use. If it requires complicated steps, it may ultimately introduce more problems. Lastly, FDA approval and clinical trials would be required to bring this product to the market. These processes take a long

time and require demonstration of numerous effective studies, so further development should focus on more achievable tasks for now. Table 3 below shows a concise summary of important considerations for future development of this work and includes estimated timelines of these goals.

Table 3: Summary of considerations for further research

<p>Short term (< 1 year)</p>	<ul style="list-style-type: none"> • Intellectual property filing • Device iterations (i.e. constructing more accurately) • Simulation to account for radial stress on vessel and more realistic loading conditions of springs
<p>Moderate term (1 – 3 years)</p>	<ul style="list-style-type: none"> • Determination of appropriate blood flow to maintain patient safety • Determination of forces present in flow-diverting stent procedures • Experimentation that considers biological effects (i.e. trade-off between necessary blood flow and number of springs)
<p>Long term (> 3 years)</p>	<ul style="list-style-type: none"> • Animal testing • FDA approval • Clinical trials

6.3: Value of this Research

While the problem of instability in flow-diverting stent delivery has been considered only briefly by previous medical device companies, if corrected, it can lead to overall improved success rates of the procedure and limit some of the complications that are typically seen during the procedure. This research has been documented in a manner

that other researchers can continue this work. The approach of this work is certainly unique since previous patents have aimed to correct the problem by other means, so it would be ideal to seek intellectual property before revealing this to the public. Once intellectual property is obtained, other researchers can build from this work. Even if they do not continue this work directly, the goal of science is to provoke thoughts within others so that they can develop their own ideas to address the need, or even address other needs with similar principles. This is a selfless ideology that researchers should take to promote the greater good of society.

Appendix A

Table 4: Raw data from Simulation A

Prescribed Radial Force (N)	Radial Displacement (mm)	Applicable Vessel Inner Diameter (mm)	Spring Constant (N/mm)	Principle Stress in Spring (N/mm ²)
0	0	4.0919	0	0
0.05	0.1514	3.7891	0.3303	55.29
0.1	0.3027	3.4865	0.3304	110.6
0.15	0.4541	3.1837	0.3303	165.9
0.2	0.6055	2.8809	0.3303	221.1
0.25	0.7568	2.5783	0.3303	276.4
0.3	0.9082	2.2755	0.3303	331.7
0.35	1.06	1.9719	0.3302	387.0
0.4	1.211	1.6699	0.3303	442.3
0.45	1.362	1.3679	0.3304	497.6
0.5	1.514	1.0639	0.3303	552.9
0.55	1.665	0.7619	0.3303	608.2

References

- [1]. Albuquerque, Cibele Gonçalves de, et al. "Deflection and flexural strength effects on the roughness of aesthetic-coated orthodontic wires." *Brazilian dental journal* 28.1 (2017): 40-45.
- [2]. "Aneurysm Clip." *Mayo Clinic*, Mayo Foundation for Medical Education and Research, <https://www.mayoclinic.org/diseases-conditions/brain-aneurysm/multimedia/aneurysm-clip/img-20007616>.
- [3]. Asri, R. I. M., et al. "Corrosion and surface modification on biocompatible metals: A review." *Materials Science and Engineering: C* 77 (2017): 1261-1274.
- [4]. Babaliaros, Vasilis, et al. "Comparison of transfemoral transcatheter aortic valve replacement performed in the catheterization laboratory (minimalist approach) versus hybrid operating room (standard approach): outcomes and cost analysis." *JACC: Cardiovascular Interventions* 7.8 (2014): 898-904.
- [5]. "Bard Medical." *Bard Medical - PTFE Coated Latex Foley Catheters*, <http://www.bardmedical.co.uk/PTFECoatedLatexFoleyCatheters>.
- [6]. "Biocompatible Adhesives." *Master Bond Biocompatible Epoxy Systems* | *MasterBond.com*, Master Bond, <https://www.masterbond.com/properties/biocompatible-adhesives>.
- [7]. Chou, Tony M, and Joey English. Methods of intracerebral implant delivery. US 20180242978A1, United States Patent and Trademark Office, 30 August 2018. *Google Patents*, <https://patents.google.com/patent/US20180242978A1/en?q=US+20180242978A1>.
- [8]. *Coefficient of Friction Analysis of Commercially Available Nitinol Guidewires*. Bard Medical, <http://m.bardmedical.com/media/3246/NICoreTechnicalPaperCOF0411.47.pdf>.
- [9]. Cowley, Alison. "A healthy future: platinum in medical applications." *Platinum Metals Review* 55.2 (2011): 98-107.
- [10]. Dotmar EPP Pty LtdMar. "Plastic Co-Efficient of Friction - Co-Efficient of Friction of Engineering Thermoplastics." *AZoM.com*, 29 Apr. 2019, <https://www.azom.com/article.aspx?ArticleID=4094>.

- [11]. Ellozy, Sharif H., et al. "Challenges of endovascular tube graft repair of thoracic aortic aneurysm: midterm follow-up and lessons learned." *Journal of vascular surgery* 38.4 (2003): 676-683.
- [12]. "Fort Wayne Metals." *Nitinol Shape Setting - Fort Wayne Metals*, <https://www.fwmetals.com/materials/nitinol/nitinol-shapesetting/>.
- [13]. Greenberg, Roy K., et al. "Should patients with challenging anatomy be offered endovascular aneurysm repair?" *Journal of vascular surgery* 38.5 (2003): 990-996.
- [14]. Higgins, John, et al. "Simulation of the Insertion of an Endostaple™ into a Vascular Stent and an Artery."
- [15]. "An Introduction to Biocompatible Plastics: Reading Plastic Machining." *Precision Plastic Machining, Die Stamping, Custom Plastics & More*, Reading Plastic, 22 Dec. 2016, <http://readingplastic.com/biocompatible-plastics/>.
- [16]. Jackson, Rubie Sue, David C. Chang, and Julie A. Freischlag. "Comparison of long-term survival after open vs endovascular repair of intact abdominal aortic aneurysm among Medicare beneficiaries." *JAMA* 307.15 (2012): 1621-1628.
- [17]. Jacobs, C R, Hayden Huang, and Ronald Y. Kwon. *Introduction to Cell Mechanics and Mechanobiology*. New York: Garland Science, 2013. Print.
- [18]. Kallmes, David F., et al. "Safety and efficacy of the Pipeline embolization device for treatment of intracranial aneurysms: a pooled analysis of 3 large studies." *Journal of neurosurgery* 127.4 (2017): 775-780.
- [19]. Khasawneh, Faisal A., and Roger D. Smalligan. "Guidewire-related complications during central venous catheter placement: a case report and review of the literature." *Case reports in critical care* 2011 (2011).
- [20]. Lake, Kelly. "Pegasus Therapeutics - Healing Kids with Aneurysms." *Indiegogo*, 23 Feb. 2015, <https://www.indiegogo.com/projects/pegasus-therapeutics-healing-kids-with-aneurysms#/>.
- [21]. Li, Guohua, et al. "Epidemiology of anesthesia-related mortality in the United States, 1999–2005." *Anesthesiology: The Journal of the American Society of Anesthesiologists* 110.4 (2009): 759-765.

- [22]. *LRX Plus Series Materials Testing Machine. LRX Plus Series Materials Testing Machine.*
- [23]. Malina, Martin, Tim Resch, and Björn Sonesson. "EVAR and complex anatomy: an update on fenestrated and branched stent grafts." *Scandinavian Journal of Surgery* 97.2 (2008): 195-204.
- [24]. Massoud, Tarik F., et al. "Endovascular treatment of multiple aneurysms involving the posterior intracranial circulation." *American journal of neuroradiology* 17.3 (1996): 549-554.
- [25]. Molyneux, Andrew J., et al. "International subarachnoid aneurysm trial (ISAT) of neurosurgical clipping versus endovascular coiling in 2143 patients with ruptured intracranial aneurysms: a randomised comparison of effects on survival, dependency, seizures, rebleeding, subgroups, and aneurysm occlusion." *The Lancet* 366.9488 (2005): 809-817.
- [26]. Molyneux, Andrew J., et al. "Risk of recurrent subarachnoid haemorrhage, death, or dependence and standardised mortality ratios after clipping or coiling of an intracranial aneurysm in the International Subarachnoid Aneurysm Trial (ISAT): long-term follow-up." *The Lancet Neurology* 8.5 (2009): 427-433.
- [27]. Mrówczyński, Wojciech, et al. "Porcine carotid artery replacement with biodegradable electrospun poly-ε-caprolactone vascular prosthesis." *Journal of vascular surgery* 59.1 (2014): 210-219.
- [28]. *Navien Intracranial Support Catheter. Covidien*, <http://neuroradialaccess.com/wp-content/uploads/2017/10/Navien-Brochure.pdf>.
- [29]. "Nitinol (Nickel Titanium)- Properties, Uses and Composition." *Chemistry Learner*, 2 Mar. 2012, <http://www.chemistrylearner.com/nitinol.html>.
- [30]. Penn, David L., Ricardo J. Komotar, and E. Sander Connolly. "Hemodynamic mechanisms underlying cerebral aneurysm pathogenesis." *Journal of Clinical Neuroscience* 18.11 (2011): 1435-1438.
- [31]. *Peripheral U.S. Product Catalog. Medtronic, Sept. 2019*, <https://www.medtronic.com/content/dam/medtronic-com/products/cardiovascular/peripheral-therapies/documents/peripheral-us-product-catalog.pdf>.

- [32]. Peyman, Gholam A., and Bharam Khoobehi. Method of performing angiography. US 5346689A, United States Patent and Trademark Office, 09 May 1992. *Google Patents*, <https://patents.google.com/patent/US5346689A/en?q=5%2c346%2c689+citation>.
- [33]. "PL100EPi." *Nautilus Systems*, 15 Feb. 2017, <https://www.nautilussys.com/products/placers/pl100epi-2/>.
- [34]. Poornejad, Nafiseh, et al. "Freezing/thawing without cryoprotectant damages native but not decellularized porcine renal tissue." *Organogenesis* 11.1 (2015): 30-45.
- [35]. "Soldering for Medical Devices." *WestTech Materials*, <https://westechmat.com/soldering-for-medical-devices/>.
- [36]. Themes, UFO. "Stents in the Treatment of Intracranial Aneurysms." *Radiology Key*, 20 Mar. 2016, <https://radiologykey.com/stents-in-the-treatment-of-intracranial-aneurysms/>.
- [37]. "Time Out for Health - Brain Aneurysm Treatment." *YouTube*, AtlantiCare, 8 Dec. 2011, <https://www.youtube.com/watch?v=8gC57E6wxf4>.
- [38]. Tsang, Anderson Chun On, et al. "Failure of flow diverter treatment of intracranial aneurysms related to the fetal-type posterior communicating artery." *Neurointervention* 10.2 (2015): 60.
- [39]. Verzini, Fabio, et al. "Appropriateness of learning curve for carotid artery stenting: an analysis of periprocedural complications." *Journal of vascular surgery* 44.6 (2006): 1205-1211.
- [40]. Wee, Ian, et al. "Carotid Access for Aortic Interventions: Genius or Madness?" *Journal*, VER Journal, 1 Sept. 2018, <https://www.verjournal.com/articles/carotid-access-aortic-interventions>.
- [41]. Yu, Simon Chun-Ho, et al. "Intracranial aneurysms: midterm outcome of pipeline embolization device—a prospective study in 143 patients with 178 aneurysms." *Radiology* 265.3 (2012): 893-901.